December 1999

Photodetachment of He⁻ in the vicinity of the He* (n=3, 4, and 5) thresholds

Chien-Nan Liu
University of Nebraska - Lincoln

Anthony F. Starace
University of Nebraska-Lincoln, astarace1@unl.edu

Photodetachment of He⁻ in the vicinity of the He* ($n=3$, 4, and 5) thresholds

Chien-Nan Liu and Anthony F. Starace

Department of Physics & Astronomy, The University of Nebraska, Lincoln, Nebraska 68588-0111
(Received 28 May 1999)

A comprehensive eigenchannel R-matrix study of photodetachment of He⁻ ($1s2s2p\,^4P^o$) is presented for the energy region of the He ($1snl\,^3l$) thresholds, where $3 \leq n \leq 5$. Over this energy region we present all partial cross sections which have been measured experimentally, including theoretical predictions for the He ($1s3p\,^3P$) partial cross section, as well as energies and widths for all resonances, and identifications of all major ones. Near the He ($n=3$) thresholds, we predict two $^4D^e$ resonances that to our knowledge have previously been neither predicted nor observed, and present results showing their effects on partial cross sections and photoelectron angular distributions; our He($1s2s\,^3S$) and He($1s2p\,^3P$) partial cross-section results are shown to be in excellent agreement with relative measurements of Klinkmüller and co-workers [Phys. Rev. A **56**, 2788 (1997); J. Phys. B **31**, 2549 (1998)]; our predicted partial cross sections and resonance energies and widths are also compared with other theoretical predictions. Near the He ($n=4$ and 5) thresholds, we predict about 30 quartet Feshbach resonances and four quartet shape resonances which have not been observed or predicted before; our predicted He ($1s3p\,^3P$) partial cross section is in excellent agreement with measurements of Kiyan *et al.* [Phys. Rev. Lett. **81**, 2874 (1998)], and we present identifications for all but one of the experimentally observed resonance features; our resonance energies and widths are also compared with other theoretically predicted results. Because resonances in the energy region considered have in general only small effects on the total photodetachment cross section, we show that alternative partial cross sections for He($1snl\,^3l$) states tend to mirror each other in the vicinity of a resonance, as predicted analytically recently by us [Phys. Rev. A **59**, R1731 (1999)]. An exceptional case is found, however, for several $^4P^e$ window resonances in the vicinity of the He ($n=4$) thresholds: the partial cross sections in the vicinity of these three resonances mimic each other. We prove analytically in an appendix that such mimicking behavior occurs whenever the Fano-Cooper profile parameter ρ^2 [Phys. Rev. A **137**, A1364 (1965)] tends to unity. [S1050-2947(99)07112-7]

PACS number(s): 32.80.Gc, 31.25.Jf

I. INTRODUCTION

The prediction of Holøien and Midtdal [1] in 1955 that the He⁻ ($^4P^o$) state is bound relative to He($2\,^3S$) has stimulated much additional work on this state [2] as well as many other theoretical studies of bound and resonance quartet states of He⁻ (e.g., see Refs. [3–14], and references therein). Only in the 1990s, however, have states involving subshells with $n \geq 3$ been studied theoretically [5–14]. In contrast to the doublet resonances of He⁻, quartet resonances have never been seen in electron scattering from ground-state He; their observation requires either electron scattering from metastable He or photodetachment from He⁻ ($^4P^o$). Hazi and Reed's theoretical predictions [15] for the photodetachment cross section of He⁻ ($^4P^o$) have been followed by numerous other theoretical photodetachment studies (e.g., see Refs. [4,8,9,12–14,16–18], and references therein.) Until 1996, theoretical works focused on low-energy photodetachment to the He ($n=2$) states [4,15–18]. Recently, interest has been shown in the high-energy photodetachment cross sections near and above the $1s$ threshold [9,12,14]. The most recent calculations examine the effects of quartet doubly excited states involving $n \geq 3$ subshells on the photodetachment cross sections [8,12–14]. However, no theoretical predictions exist for partial photodetachment cross sections to subshells with $n \geq 3$.

The earliest experimental results on He⁻ photodetachment similarly concerned only production of He ($n=2$)

states, and did not present data for doubly excited resonances associated with higher thresholds (e.g., see Refs. [19–24] and references therein). Recently, however, there have been three experimental measurements of He⁻ ($^4P^o$) photodetachment partial cross sections in the vicinity of the He ($1snl$) thresholds for $n \geq 3$ which focus on effects of quartet doubly excited resonances. Klinkmüller *et al.* [25] measured the He ($1s2s\,^3S$) partial cross section in the vicinity of a $^4S^e$ resonance associated with the He ($n=3$) threshold. The measured energy and width agree with the theoretical prediction of Ref. [8], but the width is 20% wider than predicted by Ref. [14]. Klinkmüller *et al.* [26] subsequently measured the partial photodetachment cross section for production of He ($1s2p\,^3P$) in the vicinity of three quartet Feshbach resonances associated with the He ($n=3$) thresholds. While the energy locations of these resonances agree with the most recent theoretical predictions [8,10,14], the experimentally measured widths of the two $^4P^e$ resonances differ substantially from theoretically predicted values [8,10,14]. Finally, Kiyan *et al.* [27] measured the partial photodetachment cross section for production of He ($1s3p\,^3P$) in the vicinity of the He ($n=4$ and 5) thresholds. They observed effects of 12 previously unobserved Feshbach resonances, but were unable to identify four of them owing "to a lack of theoretical input."

In this paper we present eigenchannel R-matrix [28,29] calculations for photodetachment of He ($1s2s2p\,^4P^o$) using a two-active-electron model [4]. Results for partial cross

sections in the vicinity of the He $(3 \leqslant n \leqslant 5)$ thresholds are given. We also present a complete study of all $^4S^e$, $^4P^e$, and $^4D^e$ resonances in this energy region, identify the wave functions of the corresponding doubly excited states, present density plots for the more unusual ones of them, and compare our results with available experimental partial cross-section data [25–27]. Finally, we find evidence not only of mirroring behavior [30] among our predicted partial cross sections but also of mimicking behavior, which we analyze in the Appendix.

II. THEORY

He$^-$ is treated as a two-electron system in a central field describing the He$^+$ $(1s\,^2S)$ core. Because our study is limited to an energy region well below the $1s$ detachment threshold, the two-active-electron model is valid. We choose the following LS coupling scheme,

$$\mathbf{L} = 0 + (\mathbf{l}_1 + \mathbf{l}_2), \qquad (1)$$

$$\mathbf{S} = \frac{1}{2} + (\mathbf{s}_1 + \mathbf{s}_2). \qquad (2)$$

For the He$^-$ $(1s2s2p\,^4P^o)$ initial state, electric dipole selection rules in LS coupling imply that the term values of the final state are $^4S^e$, $^4P^e$, and $^4D^e$. Therefore, the possible term values of the two-electron pairs are $^3S^e$, $^3P^e$, and $^3D^e$.

We employ the eigenchannel R-matrix method in this study. This method has proved successful in previous applications to H$^-$ and alkali-metal negative ion photodetachment [31–34]. The method has been described in detail in Ref. [32] and our method for analyzing doubly excited state resonances and their effects were described in Ref. [34]. Thus we present here only a brief overview of the eigenchannel R-matrix method and of our methods for analyzing excited, two-electron resonances.

A. Brief overview of the eigenchannel R-matrix method

The eigenchannel R-matrix method [28,29] aims to determine variationally an orthogonal and complete basis set of wave functions, the eigenchannel wave functions, at energy E whose normal logarithmic derivatives are constant across a reaction surface S enclosing a reaction volume V. For treatments of two-electron excitations, the reaction volume V is that part of six-dimensional configuration space for which both electrons lie within a sphere of radius r_0. The reaction surface S is the set of points for which $\max(r_1,r_2)=r_0$, where r_1 and r_2 are the electron distances from the nucleus. In practice, for each range of excitation energy, r_0 is chosen to be sufficiently large that the probability of both electrons being outside r_0 is negligible. Thus, r_0 has to be large enough to encompasses all possible doubly excited-state wave functions in the energy range considered. The complicated many-electron interactions within V are treated by bound state, configuration interaction (CI) techniques using a basis of independent-electron orbital wavefunctions obtained from a He$^+$ model core potential and LS coupling to represent the many-electron wave function. The model potential has the form

TABLE I. Empirical parameters for the He$^+$ model potential.

l	a_1	a_2	a_3	r_c (a.u.)
0	1.414 085	$-10.312\,226$	9.267 441	0.497 557
1	4.624 654	2.357 659	2.614 672	0.920 618
$\geqslant 2$	2.165 533	$-1.655\,991 \times 10^{-5}$	$5.391\,295 \times 10^{-2}$	1.994 665

$$V(r) = -\frac{1}{r}[Z_c + (Z - Z_c)e^{-a_1 r} + a_2 r e^{-a_3 r}]$$

$$-\frac{\alpha_c}{2r^4}(1 - e^{-(r/r_c)^3})^2. \qquad (3)$$

For our He$^-$ calculation, the nuclear charge is $Z=2$, the charge of the He$^+$ core is $Z_c=1$, and the polarizability of the He$^+$ core is given by its analytical value, 0.28125 a.u. [35]. The empirical parameters (a_1, a_2, a_3, r_c) depend on electron orbital angular momentum l and are fitted using a least-squares method to reproduce the experimentally measured energy levels of the He atom [36]. The values used in our calculation are given in Table I.

At a given energy E, one describes the wave function inside the reaction volume as a linear combination of the eigenchannel wavefunctions thus generated. Outside r_0 it is assumed there is only a single electron, and thus only single detachment processes are considered. All long-range multipole interactions in the outer region are treated numerically by close-coupling procedures in order to obtain a basis set of multichannel wave functions which describe the outgoing electron and the atomic core [32]. By thus treating the long-range multipole interactions, we are able to use much smaller values of r_0 than would otherwise be the case. By matching linear combinations of the multichannel basis functions for the inner and outer regions at the reaction surface, one can determine the exact wave function which satisfies the incoming wave boundary condition. Further details of our methods were presented in Ref. [32].

B. Identification of resonances and the corresponding doubly excited states

In order to obtain predictions for resonance energies and widths for comparison with other theoretical and experimental results, we use two different approaches, depending upon the circumstances. For an isolated resonance, we perform a least-squares fitting of our calculated partial cross section to the following resonance profile formula, which is applicable not only for total cross sections [37,38] but also for partial cross sections [39]:

$$\sigma(\epsilon) = \sigma_0 (1 + a\epsilon) \left(\frac{\epsilon^2 + b\epsilon + c}{1 + \epsilon^2} \right), \qquad (4)$$

$$\epsilon = \frac{E - E_r}{\Gamma/2}, \qquad (5)$$

where we have assumed a linear energy dependence of the background, and where E_r is the resonance energy and Γ is the resonance width. There are thus six fitting parameters: σ_0, a, b, c, E_r, and Γ. However, in the energy region

where resonances are not completely separated, we instead analyze the eigenphase sum as a function of energy. The analysis is based on the assumption that the eigenphase sum δ of a multichannel problem can be parametrized by [40,41]

$$\delta = \delta_0 + \tan^{-1}\left(\frac{\Gamma/2}{E_r - E}\right), \qquad (6)$$

where δ_0 is the eigenphase sum of the background. As in the single-channel case, the eigenphase sum increases by π in the vicinity of a resonance. Equation (6) implies that the resonance energy E_r can be determined by the location of the maximum energy derivative of δ, $d\delta/dE$. Thus δ_r, the eigenphase sum at E_r, can also be determined. The width corresponds to the energy interval between E_+ and E_-, where the eigenphase sum at these energies is $\delta_\pm = \delta_r \pm \pi/4$, respectively. Note, however, that in some instances in which resonances are located close to a threshold, the overlap of changes in the eigenphase sum with the threshold prevents us from predicting a width.

To characterize the wave functions of doubly excited resonance states, we have employed a nonstandard projection operator method which has proved successful in our studies of the Na⁻ photodetachment spectrum [34]. This method is a modification of the standard Feshbach projection operator method, and is aimed at including additional important interaction channels. According to the standard method, doubly excited states associated with the nl threshold are obtained by diagonalizing the Hamiltonian using a basis that excludes all one-electron orbitals lower in energy than nl, since such orbitals are associated with open channels. In another words, one performs a CI calculation within a subset of the configuration space. However, the degree to which electron correlation effects are faithfully described is very sensitive to the theoretical approach employed to calculate the doubly excited-state wave function.

Owing to the nondegeneracy of the atomic thresholds of He, a doubly excited resonance series converging to a given threshold often overlaps spatially with the orbitals of a lower threshold. We have found that the standard projection operator method does not explain the resonance structure very well when such overlap with lower threshold orbitals is significant. Therefore, instead of considering each nl threshold separately, we consider adjacent thresholds together and make the following modifications to the standard procedure. We apply the standard projection operator method with respect to the threshold of higher energy to define the basis states within which the Hamiltonian is diagonalized, but include also some additional configurations having the orbital of the lower-energy threshold in order to describe doubly excited states that are associated with the lower threshold. The doubly excite-state wave function obtained using this approach is then checked by a projection procedure in which cross sections are calculated using a final-state wave function that is orthogonalized to the bound state representing the resonance state. By examining its effects on the cross section, one can correlate the wave-function properties of this bound state with the resonance features in the photodetachment partial cross-section spectra. Also, proper inclusion of channel interactions is confirmed if nearby resonance features are not changed upon projecting out the bound state

under consideration. The number of additional configurations included is varied until this condition is satisfied.

In our study of Na⁻ resonances [34], we concluded that in order to obtain an accurate wave function and energy for a resonance state, one has to include all channel-coupling effects. Our nonstandard projection operator method is designed to include all important channel couplings, especially those involving interactions with other doubly excited states. Chung also showed that effects of channel coupling are important factors for the formation of resonances in negative ions [11].

Having described our method for constructing doubly excited resonance states in terms of a linear combination of two-electron configurations, we now turn to a characterization of these states. Several schemes for the classification of resonance states have been proposed which reveal the underlying symmetry of these correlated two-electron states (e.g., see Refs. [42–46] and references therein). The two schemes which focus on the angular symmetry of the two-electron states are the group theoretical $(K,T)^A$ classification [42,43] and the molecular-orbital quantum number (n_λ, n_μ, m) classification [44–46]. In this paper we indicate two-electron resonance symmetries by their $(K,T)^A$ designation. A review of the relation between the molecular orbital notation and the $(K,T)^A$ notation is given in Ref. [46].

C. Numerical details

Here we present some of the numerical details of our calculations. The radius of the R-matrix sphere, r_0, is chosen to be 180 a.u. This radius is large enough to encompass the doubly excited states in the energy range we consider. Inside the R-matrix sphere, 58 closed-type (i.e., zero at the radius r_0) and two open-type (i.e., nonzero at the radius r_0) one-electron orbital wave functions are calculated for each of the orbital angular momenta l, where $0 \leq l \leq 6$. In total, we include 2156, 1912, and 2982 closed-type, two-electron configurations in the calculation for the final-state wave function in the $^4S^e$, $^4P^e$, and $^4D^e$ channels. For each channel in which one electron can escape from the reaction volume, we include two open-type orbitals for the outer electron in addition to the closed-type basis set. For a given photon energy, in addition to all open channels, closed channels having the inner electron at the next higher principal quantum number state are also included in the calculation. Finally, the value for the electron affinity for He⁻ $(1s2s2p\ ^4P^o)$ employed in this paper is 77.518 meV [2].

III. RESULTS

A. Overview of the region from the He $(1s2s\ ^3S)$ to the He $(1s5g\ ^3G)$ thresholds

1. Total and partial photodetachment cross sections for He⁻ $(1s2s2p\ ^4P^o)$

The focus of this paper is on the photodetachment of He⁻ in the vicinities of the He ($n=3$, 4, and 5) thresholds. Our results are presented in terms of various kinds of partial cross sections, which we define here. Since the ground state of He⁻ is a $^4P^o$ state, electric dipole selection rules and LS

coupling permit only $^4L^e$ final states, where $L=0$, 1, and 2. The partial cross section $\sigma(^4L^e)$ for the $^4L^e$ final state corresponds to the process,

$$\mathrm{He}^-\ (1s2s2p\,^4P^o)+\gamma$$

$$\rightarrow \sum_{nl}^{nl(\mathrm{max})}\ \sum_{l'}\ \mathrm{He}\ (1snl\,^3l)\epsilon(nl)l'(^4L^e), \quad (7)$$

where $\epsilon(nl)$ is the kinetic energy of the detached electron when the He atom is in the state He $(1snl\,^3l)$; nl takes the values $2s \leq nl \leq 5f$ in the energy region with which we are concerned and, for a given photon energy, $nl(\mathrm{max})$ is the highest of these states that is allowed by energy conservation; also, for a given pair of values (l,L), the detached electron's orbital angular momentum l' takes all values allowed by parity and orbital angular momentum conservation.

The quartet doubly excited states of He$^-$ populated in photodetachment processes have well-defined term values $^4L^e$. It is theoretically useful to examine their effects on partial cross sections having not only a well-defined term level, but also a well-defined state of the He atom. We thus define $\sigma(nl,\,^4L^e)$ to correspond to the following process:

$$\mathrm{He}^-\ (1s2s2p\,^4P^o)+\gamma\rightarrow\sum_{l'}\ \mathrm{He}\ (1snl\,^3l)\epsilon(nl)l'(^4L^e).$$
$$(8)$$

Experiments which measure the kinetic energy of the detached electron for a given photon energy can measure the partial cross section for producing a given state of the atom. We define these partial cross sections, denoted $\sigma(nl)$, to correspond to the process,

$$\mathrm{He}^-\ (1s2s2p\,^4P^o)+\gamma$$

$$\rightarrow\sum_{l'}\ \sum_{L=0}^{2}\ \mathrm{He}\ (1snl\,^3l)\epsilon(nl)l'(^4L^e). \quad (9)$$

Finally, the total cross section σ_{total} may be expressed in terms of any of these partial cross sections, i.e.,

$$\sigma_{\mathrm{total}}=\sum_{L=0}^{2}\sigma(^4L^e)=\sum_{nl=2s}^{nl(\mathrm{max})}\sum_{L=0}^{2}\sigma(nl,\,^4L^e)$$

$$=\sum_{nl=2s}^{nl(\mathrm{max})}\sigma(nl). \quad (10)$$

In Fig. 1 we present our results for σ_{total} and for $\sigma(^4L^e)$, $0\leq L\leq 2$, over the entire photon energy range from the He $(1s2s\,^3S)$ threshold to just above the He $(1s5g\,^3G)$ threshold. Our purpose in presenting this figure is to set the energy region with which we are concerned in this paper, i.e., from just below the He $(1s3s\,^3S)$ threshold to just above the He$(1s5g\,^3G)$ threshold, into the context of the complete photodetachment spectrum of He$^-$. One sees that the largest values of the photodetachment cross sections are located near the $2s$ and $2p$ thresholds. The most prominent features in Fig. 1 are the very large peak of the well-known He $(1s2p^2\,^4P^e)$ shape resonance and the two Cooper minima in $\sigma(^4P^e)$ in the vicinity of the $n=3$ thresholds. As
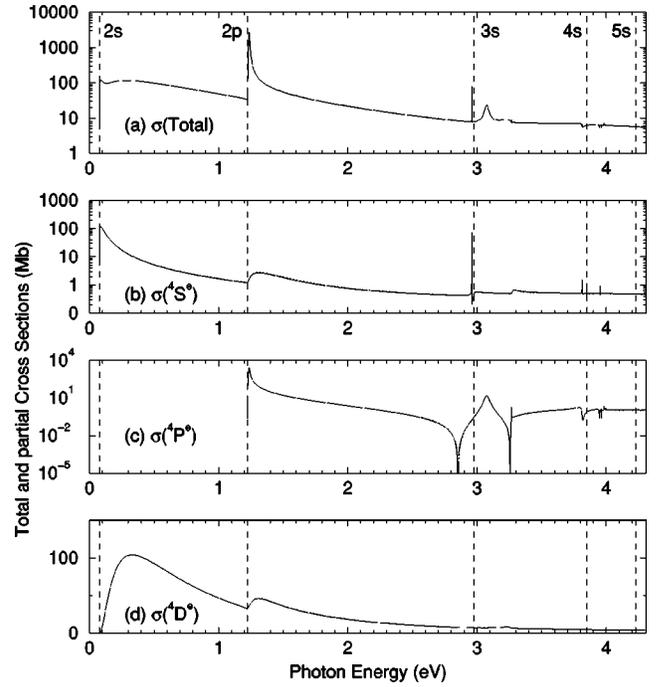

FIG. 1. Total and partial cross sections for photodetachment of He$^-$ $(1s2s2p\,^4P^o)$ for photon energies from the He$(1s2s\,^3S)$ threshold to above the He$(1s5g\,^3G)$ threshold. Present dipole length (velocity) results are indicated by the dotted (solid) lines. (a) σ_{total}. (b) $\sigma(^4S^e)$. (c) $\sigma(^4P^e)$. (d) $\sigma(^4D^e)$.

the region below the $n=3$ thresholds has already been extensively studied both experimentally [19–24] and theoretically [4,8,14–18], and as our results are consistent with this prior work, we shall omit further discussion of this low-energy region. Our focus, rather, is on the resonance structures in the vicinities of the He $(n=3,\ 4,\ \mathrm{and}\ 5)$ thresholds.

In Figs. 2 and 3, we present an overview of our results of He$^-$ photodetachment in the energy regions near the He $(n=4)$ and He$(n=5)$ thresholds respectively. Figures 2(a) and 3(a) show σ_{total} in these two energy regions. Its decomposition into the three partial cross sections $\sigma(^4L^e)$ corresponding to different total orbital angular momentum states are presented in Figs. 2(b)–2(d) and 3(b)–3(d). The magnitudes of $\sigma(^4L^e)$ for different values of L reflect the multiplicity of different final state channels [cf. Eq. (7)]. Note also that most of the resonances appearing in this energy region have minima which are only small dips in the total cross section. (Note that the ordinates in Figs. 2 and 3 do not always start at zero.) Therefore, only a small fraction, denoted by ρ^2, of the total cross section interacts with each of the resonances [47]. This kind of resonance behavior is expected for the total photodetachment cross section in the energy region for which high levels of excitation of the residual atom are possible.

2. Mirroring and mimicking behaviors

It has been proved that when $\rho^2\rightarrow 0$, mirroring behavior of the partial cross sections in the vicinity of a resonance is to be expected [30]. More specifically, it is proved in Ref. [30] that for an isolated resonance for which $\rho^2\rightarrow 0$ (i.e., for which the maximum fractional depth in the total cross section approaches zero), then for any arbitrary division of the
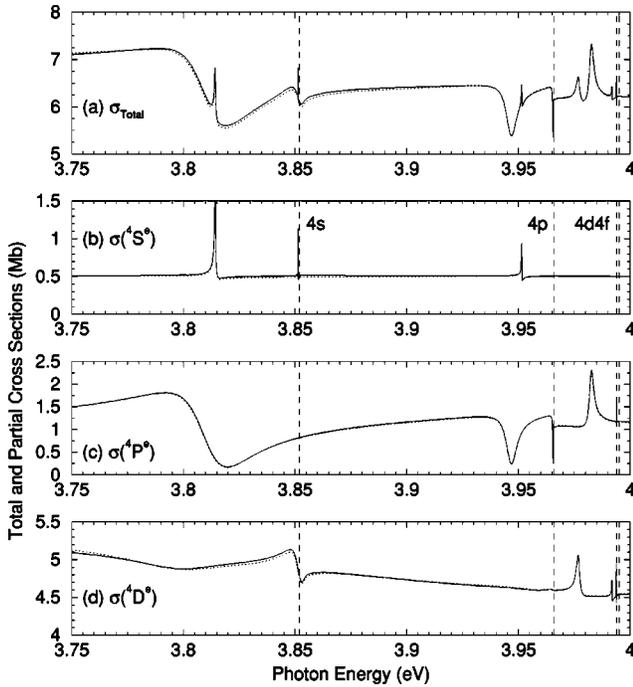
FIG. 2. Total and partial cross sections for photodetachment of He⁻ vs photon energy in the energy region near the He ($n=4$) thresholds. Present dipole length (velocity) results are indicated by dotted (solid) lines. (a) σ_{total}. (b) $\sigma(^4S^e)$. (c) $\sigma(^4P^e)$. (d) $\sigma(^4D^e)$. The vertical dashed lines indicate the locations of the He ($1snl\,^3L$) thresholds for $4s \leq nl \leq 4f$.
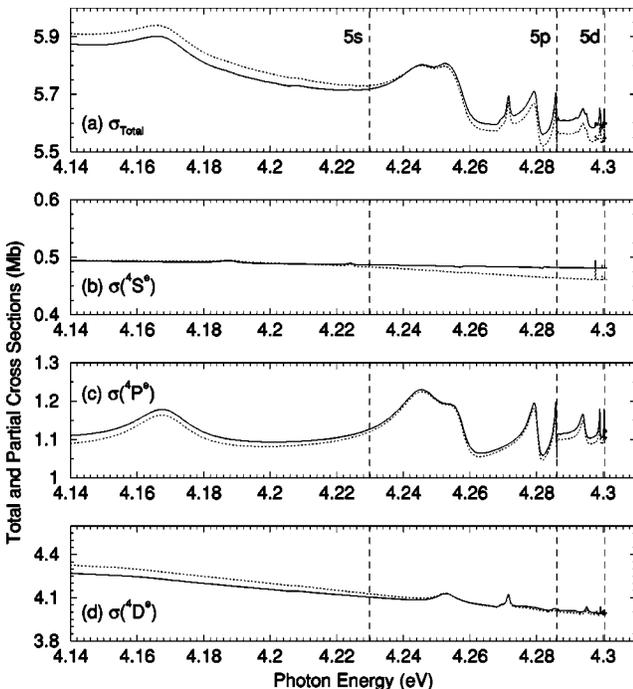

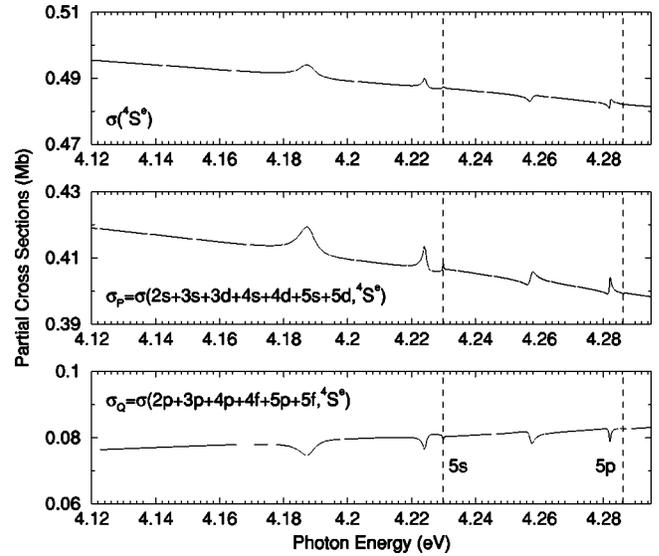FIG. 3. Same as Fig. 2 in the energy region region near the He ($n=5$) thresholds.

FIG. 4. Mirroring behavior in the $^4S^e$ partial cross sections in the region of the He ($n=5$) thresholds. (a) $\sigma(^4S^e)$. (b) $\sigma_P = \Sigma_{nl}\sigma(nl,^4S^e)$, for $2s \leq nl \leq 5d$ and l even. (c) $\sigma_Q = \Sigma_{nl}\sigma(nl,^4S^e)$, for $2p \leq nl \leq 5f$ and l odd. The vertical dashed lines indicate the locations of the He ($1snl\,^3L$) thresholds for $nl = 5s$ and $5p$. Note that $\sigma(^4S^e) = \sigma_P + \sigma_Q$ and that σ_P and σ_Q mirror one another relative to changes in $\sigma(^4S^e)$ in the vicinity of the resonances, as predicted analytically in Ref. [30].

partial cross sections into two groups, designated P and Q, so that $\sigma_{total} = \sigma_P + \sigma_Q$, σ_P, and σ_Q will vary in the vicinity of the resonance in a mirrorlike way, with increases (decreases) in σ_P matched by decreases (increases) in σ_Q. This mirroring is exact relative to whatever changes occur in σ_{total} in the vicinity of the resonance. Figure 4 illustrates this effect. One sees from Fig. 4(a) that $\sigma(^4S^e)$, which is the total $^4S^e$ cross section, shows minimal evidence of resonance structure, indicating that $\rho \approx 0$, so that the predictions of Ref. [30] are applicable to this case. Thus when we split $\sigma(^4S^e)$ into two groups, a group P equal to the sum of all $\sigma(nl, ^4S^e)$ for l even and a group Q equal to the sum of all $\sigma(nl, ^4S^e)$ for l odd, as shown in Fig. 4, we see that σ_P and σ_Q mirror each other in the vicinity of the $^4S^e$ doubly excited resonances relative to the changes in σ_{total} in the vicinity of the resonances. If the effects of the resonances on $\sigma(^4S^e)$ were nil, then the mirroring of σ_P and σ_Q would be exact [30]. Note that the three panels in Fig. 4 are plotted on the same scale in order to facilitate comparisons of changes in the vicinities of the resonances. Note also that, according to Ref. [30], the division of σ_{total} into two groups P and Q is quite arbitrary: results similar to those shown in Fig. 4 may be found for other choices for P and Q.

Figure 5 shows that such mirroring behavior happens to occur often in the individual partial cross sections. We see that the $\sigma(4p, ^4S^e)$ and $\sigma(4d, ^4S^e)$ partial cross sections, for example, are nearly mirror images of each other in the vicinity of resonances. While these resonances are not prominent in the partial cross section $\sigma(^4S^e)$ [cf. Fig. 4(a)], the $\sigma(4l, ^4S^e)$ partial cross sections shown in Fig. 5 are dominated by the doubly excited resonances, exhibiting such interference effects as asymmetric peaks and, in some cases, nearly zero minima, which possibility was also predicted in Ref. [30].

In contrast to the typical case that for high values of nl, doubly excited resonance states have $\rho^2 \rightarrow 0$, in Fig. 2(c) one sees three notable exceptions in the $\sigma(^4P^e)$ partial cross section in the vicinity of the $4s$ and $4p$ thresholds. These ex-
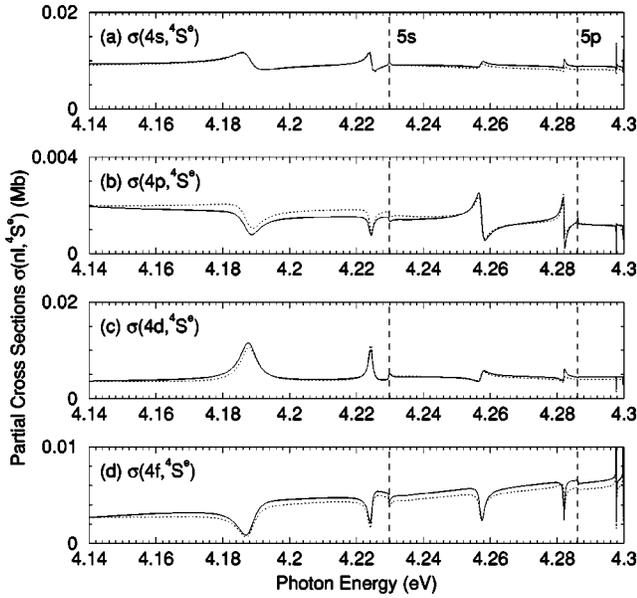
FIG. 5. $\sigma(nl, {}^4S^e)$ partial cross sections in the vicinity of the He ($n=5$) thresholds. (a) $\sigma(4s, {}^4S^e)$. (b) $\sigma(4p, {}^4S^e)$. (c) $\sigma(4d, {}^4S^e)$. (d) $\sigma(4f, {}^4S^e)$. The vertical dashed lines indicate the locations of the He ($1snl\,{}^3L$) thresholds for $nl=5s$ and $5p$.

ceptional doubly excited resonances are located at 3.81, 3.945, and 3.965 eV, and have nearly zero minima, indicating a correlation index ρ^2 close to unity [47]. We show in the Appendix that, for a resonance having $\rho^2 \rightarrow 1$, variations of different partial cross sections in the vicinity of the resonance are *in phase*. That is, they mimic one another in the neighborhood of the resonance. The $\sigma(nl, {}^4P^e)$ partial cross sections in the neighborhood of these three resonances are shown in Fig. 6 to illustrate such mimicking behaviors.

In the following sections, detailed analyses of the doubly excited resonances in the vicinity of the He ($n=3$, 4, and 5) thresholds are presented. We focus on $\sigma(nl)$ partial cross sections, for two reasons. First, these partial cross sections are more sensitive to the resonances than is the total cross section. Second, experimental data are available for comparison [25–27].

B. He$^-$ photodetachment near the He ($n=3$) thresholds

As described in Sec. I, Klinkmüller *et al.* [25] measured the $\sigma(2s)$ partial cross section below the He ($1s3s\,{}^3S$) threshold in the vicinity of a ${}^4S^e$ resonance, while Klinkmüller *et al.* [26] measured the $\sigma(2p)$ partial cross section in the photon energy range 2.9 eV $\leqslant \hbar\omega \leqslant$ 3.3 eV and observed three Feshbach resonances. For each of the four resonance measurements, resonance energies and widths were obtained by fitting the measured partial cross sections to the parameterized Shore profile formula [38]. While their resonance energies agree more or less with earlier theoretical results, two of the reported resonance widths differ noticeably from all theoretical values (cf. Table 1 in Ref. [26]). Furthermore, recent R-matrix calculations of Ramsbottom and Bell [14] for the photodetachment partial cross sections $\sigma(2p)$ in this energy region also predicted widths for the three resonances which disagree with the measured values [26]. Therefore, it is of some interest to examine these resonances in more detail.
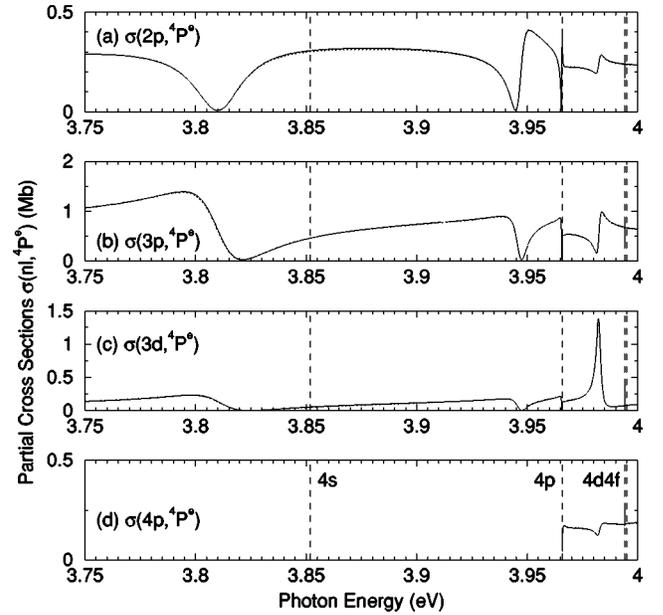

FIG. 6. $\sigma(nl, {}^4P^e)$ partial cross sections in the vicinity of the He ($n=4$) thresholds. (a) $\sigma(2p, {}^4P^e)$. (b) $\sigma(3p, {}^4P^e)$. (c) $\sigma(3d, {}^4P^e)$. (d) $\sigma(4p, {}^4P^e)$. The vertical dashed lines indicate the locations of the He ($1snl\,{}^3L$) thresholds for $4s \leqslant nl \leqslant 4f$. Note the mimicking behavior of the resonances located at $\hbar\omega=3.81$, 3.945, and 3.965 eV.

Figure 7 shows our results for the $\sigma(2p)$ partial cross section in the neighborhood of He ($n=3$) thresholds as well as the partial cross sections $\sigma(2p, {}^4L^e)$ associated with different total orbital angular momenta. All three resonances that have been identified experimentally are indeed the most
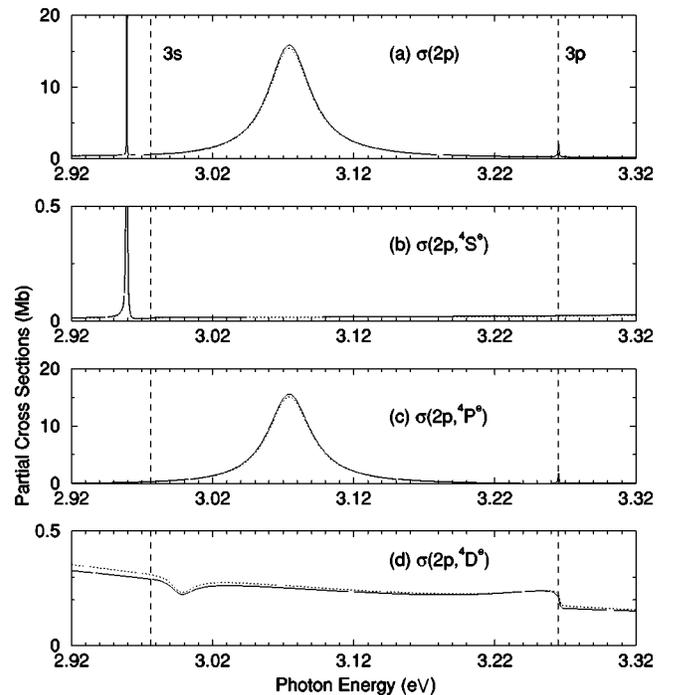

FIG. 7. Partial cross sections near the He ($n=3$) thresholds. (a) $\sigma(2p)$. (b) $\sigma(2p, {}^4S^e)$. (c) $\sigma(2p, {}^4P^e)$. (d) $\sigma(2p, {}^4D^e)$. The vertical dashed lines indicate the locations of the He ($1snl\,{}^3L$) thresholds.
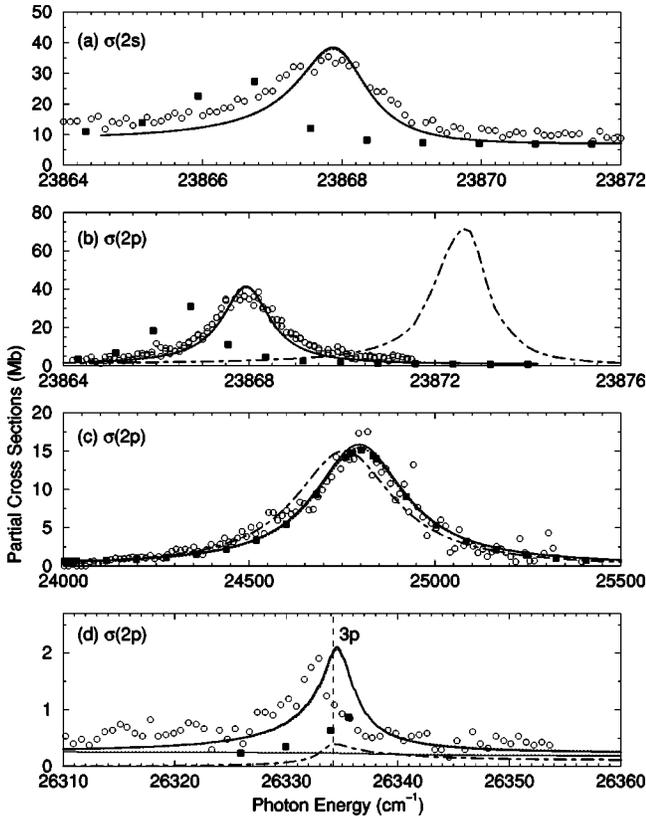
FIG. 8. Partial cross sections in the vicinity of the $^4S^e$ and $^4P^e$ resonances near the He ($n=3$) thresholds. (a) $\sigma(2s)$ near the $1s3s4s\,^4S$ resonance. (b) $\sigma(2p)$ near the $1s3s4s\,^4S$ resonance. (c) $\sigma(2p)$ near the $1s3p^2\,^4P$ resonance. (d) $\sigma(2p)$ near the $1s3pnp\,^4P$ resonance. Dark solid (dotted) curves indicate the present results in dipole velocity (length) approximation; dot-dashed lines indicate predictions of Ramsbottom and Bell [14]; solid squares indicate the predictions of Xi and Fischer [8]; and open circles indicate the relative measurements of Klinkmüller and co-workers [25,26], whose magnitudes are fitted to our predictions. The light solid (dotted) line in the lower part of (d) is our dipole velocity (length) result upon projecting out the effect of the $1s3pnp$ ($^4P^e$) resonance.

prominent features in this energy region. The decomposition of the $\sigma(2p)$ partial cross section into its $\sigma(2p,\,^4L^e)$ partial cross-section components, however, reveals in our calculations a $^4D^e$ resonance at a photon energy of 2.997 eV in $\sigma(2p,\,^4D^e)$ that is not visible in the $\sigma(2p)$ partial cross section. The only prior prediction of a $^4D^e$ resonance near this energy region of which we are aware stems not from studies of photodetachment, but rather from a study by Oberoi and Nesbet [48] of inelastic e^--He scattering. In fact, our more detailed analysis reveals there is an additional $^4D^e$ resonance, located in the vicinity of the He ($1s3p\,^3P$) threshold. In what follows, we discuss first our predictions for the experimentally observed $^4S^e$ and $^4P^e$ resonances, and then discuss our two theoretically predicted $^4D^e$ resonances, which have yet to be observed experimentally.

1. $^4S^e$ and $^4P^e$ resonances

Figure 8 shows the resonance profiles predicted by our calculated $\sigma(2s)$ and $\sigma(2p)$ partial cross sections, and compares them with the relative experimental measurements

[25,26], whose magnitudes are scaled to our predictions. We have performed a least-squares fitting of our results to a resonance profile formula [cf. Eqs. (4) and (5)] in order to obtain the resonance energies and widths. Fitting our results to a parametrized resonance profile is justified for these resonances, since they appear in this energy region to be well separated, and hence may be treated theoretically as isolated. Results of our fitting are presented in Table II along with other theoretical and experimental results. Each of the resonance states listed in Table II shows strong configuration mixing; thus the configuration designations employed indicate merely the dominant configuration component. Note, however, that instead of using the $1s3p4p\,^4P^e$ configuration designation for the resonance at $\hbar\omega=3.265$ eV, we designate it as $1s3pnp\,^4P^e$ because this state does not have a strong $1s3p4p$ component, at least in our calculations. We discuss each of the three resonances for which there are experimental data in turn.

The narrow $1s3s4s\,^4S^e$ resonance at $\hbar\omega=2.959$ eV shown in Figs. 7(a) and 7(b) affects both the $\sigma(2s)$ and $\sigma(2p)$ partial cross sections, and is observed in both experiments by Klinkmüller and co-workers [25,26]. Comparisons of our predictions for $\sigma(2s)$ and $\sigma(2p)$ in the vicinity of this resonance with the experimental measurements are shown in Figs. 8(a) and 8(b). As shown in Table II, all theoretical predictions for the energy location of this resonance (including ours) agree (more or less) with the measured values. Our width of 0.154 eV, however, is closer to the predictions of Brandefelt and Lindroth [13] and Ramsbottom and Bell [14], who each predict 0.16 eV, than to the predictions of 0.18eV–0.19 eV of Xi and Fischer [8], which agree with the measured width of 0.19–0.20 eV [25,26]. The predictions of Xi and Fischer [8] for both $\sigma(2s)$ and $\sigma(2p)$ as well as those of Ramsbottom and Bell [14] for $\sigma(2p)$ in the vicinity of the $^4S^e$ resonance are also shown in Figs. 8(a) and 8(b). The energy prediction of Xi and Fischer [8] for this resonance differs from the experimentally measured value by only 0.18 meV while that of Ramsbottom and Bell [14] differs by only 0.57 meV, but because the resonance has a width of only ≈ 0.2 meV, this difference is quite noticeable on the cm^{-1} energy scale employed in Figs. 8(a) and 8(b). One sees that Ref. [8]'s peak heights in both $\sigma(2s)$ and $\sigma(2p)$ are approximately 30% lower than ours, and that the peak shape appears less symmetric than ours. One sees also that Ref. [14]'s prediction for the peak height of $\sigma(2p)$ at the predicted resonance position is more than 50% greater than our predicted value, although the peak shape is quite similar to ours.

Our results for $\sigma(2p)$ in the vicinity of the $1s3p^2(^4P^e)$ resonance are shown in Fig. 8(c) together with the experimental data [26] and the theoretical predictions of both Xi and Fischer [8] and Ramsbottom and Bell [14]. As may be seen from Table II, the experimentally measured location for this resonance at $\hbar\omega=3.072$ eV lies between the most recent theoretical predictions, namely, the value $\hbar\omega=3.074$ eV predicted by us as well as by Xi and Fischer [8] on the one hand, and the value $\hbar\omega=3.069$ predicted by Bylicki [10] and Ramsbottom and Bell [14] on the other hand. As shown in Fig. 8(c), our prediction for the peak height of $\sigma(2p)$ in the vicinity of the $1s3p^2(^4P^e)$ resonance agrees quite well with those predicted both by Xi and Fischer [8]

TABLE II. Resonance energies and widths of He$^-$ near the He $(n=3)$ thresholds. The resonance energies are determined with respect to the He$^-$ $(1s2s2p\ {}^4P)$ state.

	$1s3s4s\ {}^4S^e$		$1s3p^2\ {}^4P^e$		$1s3pnp\ {}^4P^e$		$1s3snd\ {}^4D^e$		$1s3pnp\ {}^4D^e$
	E_0 (eV)	Γ (meV)	E_0 (eV)	Γ (meV)	E_0 (eV)	Γ (meV)	E_0 (eV)	Γ (meV)	E_0 (eV)
Theory									
This work									
Length form	2.959 248	0.154	3.074 104	35.507	3.265 076	0.564	2.997 437	19.290	3.265 775[a]
Velocity form	2.959 248	0.154	3.074 004	35.590	3.265 076	0.565	2.997 369	19.540	
Oberoi and Nesbet[b]							2.82	10	
Hazi and Reed[c]			3.10						
Davies and Chung[d,e]			3.082 242	33					
Themelis and Nicolaides[f,e]			3.091 983	34.6					
Xi and Fischer[g]									
Length form	2.959 07	0.19	3.074 070	37.37	3.265 54	1.30			
Velocity form	2.959 08	0.18	3.074 071	37.37	3.265 47	1.31			
Bylicki[h,e]			3.069 697	37	3.260 259	2.45			
Brandefelt and Lindroth[i]	2.959 24	0.16							
Ramsbottom and Bell[j]	2.959 83	0.16	3.069 6	40.22	3.264 97	0.7715			
Experiment									
Klinkmüller et al.[k]	2.959 255	0.19							
Klinkmüller et al.[l]	2.959 260	0.20	3.072	50	3.264 87	0.61			

[a]Obtained from an eigenphase sum analysis.
[b]Reference [48], p. 2974.
[c]Reference [15], p. 2269.
[d]Reference [5], Table 1.
[e]These values for the energies and widths are determined using the energy of He$^-$ $(1s2s2p\ {}^4P^o)$, $-2.177\,877\,25$ a.u., and the conversion factor 1 a.u.$= 27.211\,396$ eV.
[f]Reference [7], Table 4.
[g]Reference [8], Table V.
[h]Reference [10], Table 2.
[i]Reference [13], Table IV.
[j]Reference [14], Tables 6–8.
[k]Reference [25], Table II.
[l]Reference [26], Table 1.

and by Ramsbottom and Bell [14]. Finally, Table II shows that all theoretical predictions for the width of this resonance lie in the range 33–40 meV, while the experimentally fitted width is 50 meV [26]. Figure 8(c), however, shows that our predictions for $\sigma(2p)$ as well as those of Refs. [8] and [14] appear to be in quite good agreement with the relative experimental data [26].

Finally, our results for $\sigma(2p)$ in the vicinity of the $1s3pnp(^4P^e)$ resonance are shown in Fig. 8(d) together with the relative experimental data [26] and the predictions of both Xi and Fischer [8] and Ramsbottom and Bell [14]. As shown in Table II, whereas the experimental value for the location of this resonance agrees with all of the theoretical predictions except for that of Ref. [10], the experimentally measured width of 0.61 meV agrees best with our prediction of 0.56–0.57 meV; the other predicted widths range from 26% to 300% larger. It should be noted that this resonance is very close to the He $(1s3p\ {}^3P)$ threshold at 3.264 98 eV [36]. However, while the experimentally measured resonance energy lies below the threshold, all theoretical predictions find the resonance above the He $(1s3p\ {}^3P)$ threshold. (Note that although the predicted resonance energies of Bylicki [10] and Ramsbottom and Bell [14] appear to be lower than the threshold energy given above, they are higher than the

threshold energies used in the respective calculations: cf. Table 1 in Ref. [10] and p. 1329 of Ref. [14].) Regarding the peak height of $\sigma(2p)$ in the vicinity of this resonance, our predicted value is more than a factor of 2 larger than that predicted by Ref. [8] and more than a factor of 4 larger than that predicted by Ref. [14].

Typically when a resonance lies below a threshold it is called a "Feshbach" resonance, whereas when it lies above it is called a "shape" resonance [49]. Thus for the $1s3pnp$ $(^4P^e)$ resonance, the question arises as to whether it is a Feshbach or a shape resonance. Nicolaides et al. [50] argued that in determining the nature of a resonance, the question of its location relative to nearby thresholds is not physically significant. We agree. In order to be sure that the doubly excited state obtained in our bound-state calculation does actually account for the resonance feature we predict in our full calculations near the He $(1s3p\ {}^3P)$ threshold, we have orthogonalized our final-state wave function to the doubly excited state. The result is the light solid (dotted) line in Fig. 8(d), representing our dipole velocity (length) result. One sees that when we thus project out the doubly excited state, the $\sigma(2p)$ partial cross section is visually flat, with no evidence of any resonance structure. This gives us confidence that the doubly excited state we calculate describes all
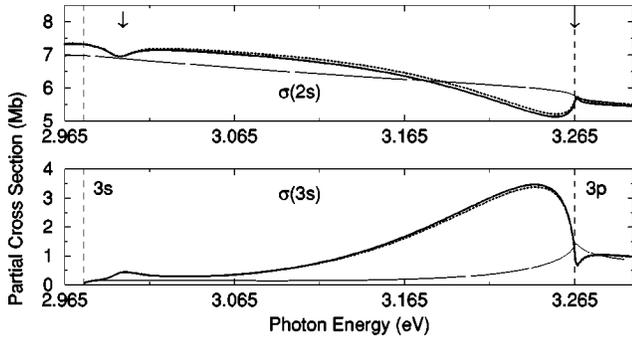
FIG. 9. Partial cross sections near the He $(n=3)$ thresholds. (a) $\sigma(2s)$. (b) $\sigma(3s)$. The vertical dashed lines indicate the locations of the He $(1snl\,^3l)$ thresholds. The dark solid (dotted) curve indicates our results in dipole velocity (length) approximation. The light solid curves indicate the effect on the dipole velocity cross section of orthogonalizing our $^4D^e$ final-state wave function to both of our predicted $^4D^e$ resonance states shown in Table II, whose energy positions are indicated by the arrows.

observed resonance features in our full calculations for $\sigma(2p)$, shown by the dark solid (dotted) line in Fig. 8(d).

2. $^4D^e$ resonances

Our calculations predict two $^4D^e$ resonances in the vicinity of the He $(n=3)$ thresholds, neither of which has been observed experimentally. As indicated in Table II, the first is located at $\hbar\omega=2.9974$ eV, just above the He $(1s3s\,^3S)$ threshold, and the second is located at $\hbar\omega=3.2658$ eV, just below the He $(1s3p\,^3P)$ threshold. The resonance energy and width of the first resonance shown in Table II are obtained by fitting the $\sigma(2p,\,^4D^e)$ partial cross section to a parametrized resonance profile. However, the profile fitting is not successful for the second resonance because it overlaps with the He $(1s3p\,^3P)$ threshold. Instead, we obtain the resonance energy for the second resonance by analyzing the eigenphase sum. Since the second resonance overlaps with the He $(1s3p\,^3P)$ threshold, we are not able to determine its width. Oberoi and Nesbet [48] found ''evidence of a $^4D^e$ resonance'' in the energy region of the He $(1s3s\,^3S)$ threshold, but their energy location and width (cf. Table II) are very different from the results we have obtained.

Experimental observation of these two $^4D^e$ resonances will require measurements of cross sections other than $\sigma(2p)$ in the energy region between the He $(1s3s\,^3S)$ and He $(1s3p\,^3P)$ thresholds. Indeed, as shown in Fig. 7, only in the $\sigma(2p,\,^4D^e)$ component of $\sigma(2p)$ are the effects of these two resonances visible, the first producing a window feature and the second producing a shoulder feature. However, $\sigma(2p)$ is dominated by the $\sigma(2p,\,^4P^e)$ component so that these two resonances are not visible. In contrast, as shown in Fig. 9, both the $\sigma(2s)$ and the $\sigma(3s)$ partial cross sections are significantly affected by these two resonances since there is no $^4P^e$ component in either $\sigma(2s)$ or $\sigma(3s)$. That these two resonances are responsible for most of the structure in $\sigma(2s)$ and $\sigma(3s)$ is shown by the curves in Fig. 9, giving the result of orthogonalizing our $^4D^e$ final-state wave function to both of these two resonances.

Alternatively, another way to observe these two resonance states is by measuring the photoelectron asymmetry parameter $\beta(nl)$ for the process
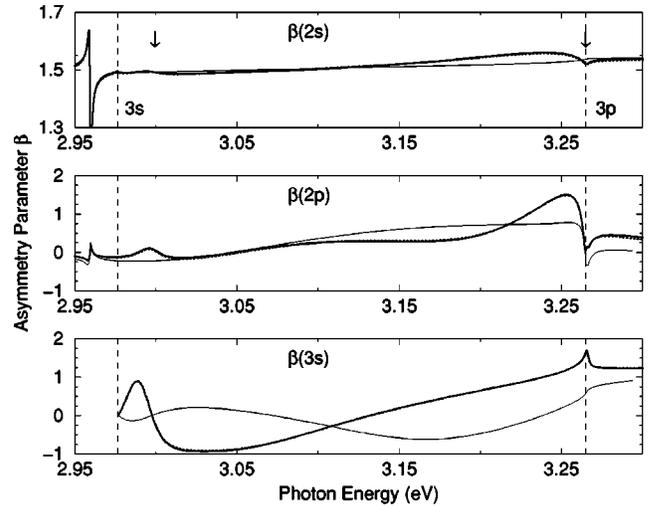

FIG. 10. Photoelectron angular distribution asymmetry parameters $\beta(nl)$. (a) $\beta(2s)$. (b) $\beta(2p)$. (c) $\beta(3s)$. The dark solid (dotted) curve indicates our results in dipole velocity (length) approximation. The light solid curves indicate the effect on the dipole velocity result of orthogonalizing our $^4D^e$ final-state wave function to both of our predicted $^4D^e$ resonance states shown in Table II, whose energy positions are indicated by the arrows.

$$\text{He}^-\ (1s2s2p\,^4P^o)+\gamma\rightarrow\text{He}\ (1snl\,^3l)+e^-. \quad (11)$$

Our predictions for $\beta(2s)$, $\beta(2p)$, and $\beta(3s)$ are shown in Fig. 10. In contrast to our results for $\sigma(nl)$, which showed that $\sigma(2s)$ and $\sigma(3s)$ were most significantly affected by our two predicted $^4D^e$ resonances (cf. Figs. 7 and 9), Fig. 10 shows that for the photoelectron angular distribution, $\beta(2p)$ and $\beta(3s)$ are most significantly affected.

Radial and angular density plots of the two $^4D^e$ resonance states we predict are shown in Fig. 11. Each state's probability density is plotted in three different ways: in (r_1,r_2) coordinates; in hyperspherical angular coordinates (α,θ_{12}); and in prolate spheroidal coordinates (μ,λ). The angular plots are made at a particular value of the radius $R\equiv\sqrt{r_1^2+r_2^2}$, which is $R=20$ a.u. for the first state and $R=32$ a.u. for the second one. From these density plots we may classify the two resonance states using the group theoretical notation $_N(K,T)^A$ as $_3(2,0)^+$ and $_3(2,0)^-$, indicating that they have no nodes in θ_{12} or λ, and that the first resonance state has an antinode at $r_1=r_2$ while the second has a node there.

C. He⁻ photodetachment near the He $(n=4)$ thresholds

Figure 12(a) shows our results for the $\sigma(3p)$ partial cross section in the vicinity of the He $(n=4)$ thresholds together with the recent relative experimental results of Kiyan et al. [27], which have been normalized to our theoretical predictions. (Note that the experimental data actually include not only the He $(1s3p\,^3P)+e^-(\epsilon p)$ channel, as stated in Ref. [27], but also the He $(1s3p\,^3P)+e^-(\epsilon f)$ channel, which contributes to $\sigma(^4D^e)$, since the experiment did not distinguish these two channels.) The letters **a**–**f** in Fig. 12(a) are the labels used in the experimental paper [27] for the observed resonances. Agreement between the theoretical and experimental results is good, except for some amplitude discrepancies. We have checked our theoretical predictions
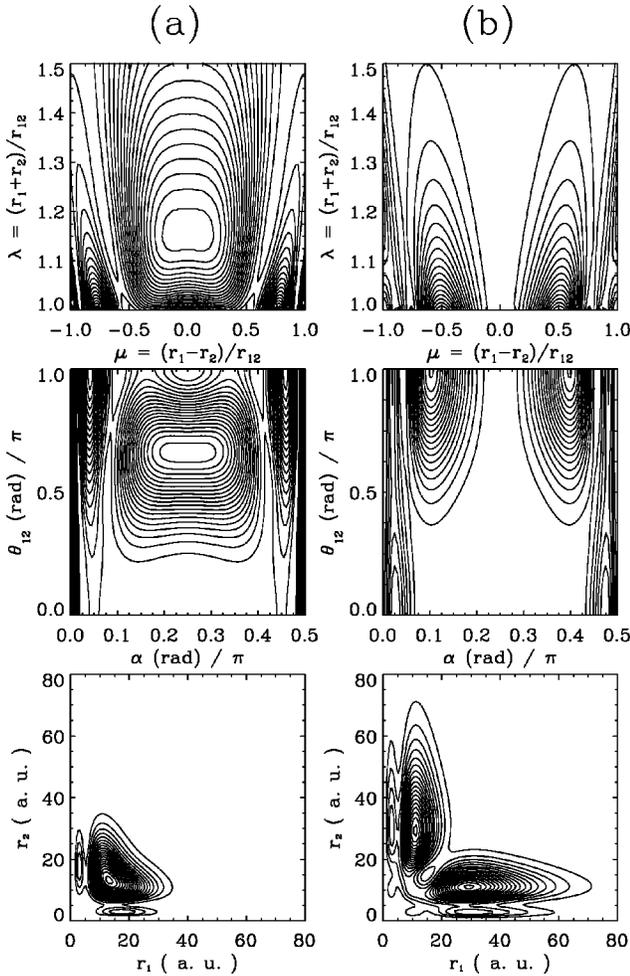
(a)   (b)

FIG. 11. Density plots for He$^-$ $^4D^e$ resonance states near the He ($n=3$) thresholds. (a) $_3(2,0)^+$ state located at $\hbar\omega = 2.9974$ eV. (b) $_3(2,0)^-$ state located at $\hbar\omega = 3.2658$ eV. The top panels are plotted in prolate spheroidal coordinates λ and μ at a value of $R \equiv \sqrt{r_1^2+r_2^2}$ which corresponds to the maximum wave-function amplitude: (a) $R=20$ a.u. (b) $R=32$ a.u. The middle panels are plotted in hyperspherical coordinates θ_{12} and $\alpha \equiv \tan^{-1}(r_2/r_1)$ at the same values of R. The bottom panels are plotted in (r_1,r_2) coordinates with angular variables averaged.

carefully for convergence in this energy region. The relative measurements were made using a parallel beam experimental arrangement [27].

The $\sigma(3p)$ partial cross section is the sum of three partial cross sections $\sigma(3p,{}^4L^e)$, which are presented in Figs. 12(b)–12(d). By decomposing the $\sigma(3p)$ cross section in this way, it is possible theoretically to accurately characterize the term value of the doubly excited states that are responsible for the observed resonance structures. Furthermore, our analysis of the eigenphase sum reveals many resonances that are neither identified in the experimental measurements [27] nor in previous theoretical works [7,8,10]. A complete list of all $^4S^e$, $^4P^e$, and $^4D^e$ resonances that our calculations predict in the vicinity of the He ($n=4$ and 5) thresholds are presented in Tables III–V together with their energies and widths. We also calculate the cross section that results after removing a specific doubly excited state, thus verifying that it alone accounts for the resonance features predicted as well as illustrating its effects. Therefore, we can correlate the pre-
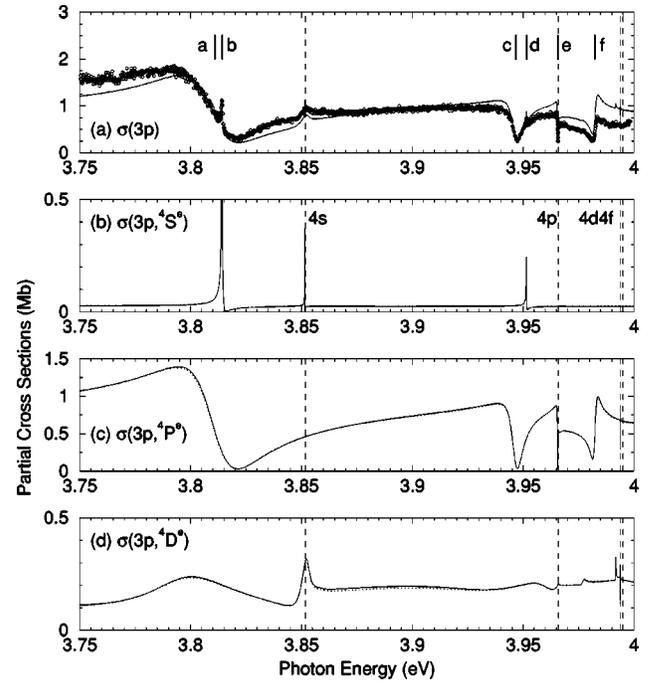

FIG. 12. Partial cross sections in the vicinity of He ($n=4$) thresholds. (a) $\sigma(3p)$. (b) $\sigma(3p,{}^4S^e)$. (c) $\sigma(3p,{}^4P^e)$. (d) $\sigma(3p,{}^4D^e)$. Curves: present results in dipole length (dotted) and velocity (solid) gauges. Circles: relative experimental measurements of Kiyan *et al.* [27] normalized to our theoretical predictions. Labels **a**–**f** in (a) are those used in Ref. [27]. The vertical dashed lines indicate the locations of the He ($1snl\,{}^3l$) thresholds.

dicted cross section features of these resonances with the $_N(K,T)^A$ character of the corresponding doubly excited states.

Some general observations can be made regarding the spectra presented in Fig. 12. First, although the $\sigma({}^4D^e)$ partial cross section dominates the total cross section (cf. Fig. 2), it is nevertheless the $\sigma(3p,{}^4P^e)$ partial cross section which gives the largest contribution to the $\sigma(3p)$ partial cross section, and the $^4P^e$ resonances are the ones which dominate the $\sigma(3p)$ spectrum. Figure 12(b) shows that there is a series of very narrow $^4S^e$ resonances on top of an almost constant background. The $^4D^e$ resonances, seen best in Fig. 12(d), are less prominent compared with resonances of the other two symmetries, and it is difficult to discern the $^4D^e$ resonances in the composite $\sigma(3p)$ partial cross section shown in Fig. 12(a). In what follows, we discuss the $^4S^e$, $^4P^e$, and $^4D^e$ resonances we predict in this energy region in more detail.

Figure 12(b) clearly shows three narrow isolated peaks in the $\sigma(3p,{}^4S^e)$ partial cross section, indicating the presence of three $^4S^e$ resonances. While two of them were labeled by Kiyan *et al.* [27] (i.e., **b** and **d**), only the lower-energy one is identified in Ref. [27] as a $^4S^e$ resonance. In our analysis, using the methods described in Sec. II B above, we are able to characterize these three $^4S^e$ resonances. The three doubly excited states are obtained by diagonalizing a Hamiltonian that excludes all configurations involving orbitals below $4p$ except $4s4p$, $4s5p$, and $4s6p$. The effect of each of these three resonances on the $\sigma(3p,{}^4S^e)$ partial cross section is shown in Fig. 13. The narrow resonance at 3.814 225 eV

TABLE III. $^4S^e$ resonance energies and widths of He⁻ in the energy region near the He $(n=4)$ and He $(n=5)$ thresholds.

$_N(K,T)^A$	Present results $\hbar\omega$ (eV)	Γ (meV)	Label	Experiment[a] $\hbar\omega$ (eV)	Γ (meV)	Other theory[b] $\hbar\omega$ (eV)	Γ (meV)
	3.268 263[c]						
$_4(3,0)^-$	3.814 225	0.8	**b**	3.814 29(9)	0.8(2)	3.814 19	0.73
$_4(3,0)^-$	3.851 397						
$_4(1,0)^-$	3.951 457	0.2	**d**	3.9515(1)	0.3(2)	3.951 58	0.15
	3.966 137[c]						
	3.994 009						
	4.187 816	6.9				4.187 79	5.5
	4.224 291	1.4					
	4.257 274	2.1					
	4.281 951	0.6					
	4.286 247[c]						
	4.297 739	0.04					
	4.299 666						

[a]I. Yu. Kiyan, U. Berzinsh, D. Hanstorp, and D. J. Pegg, Ref. [27].
[b]N. Brandefelt and E. Lindroth, Ref. [13].
[c]Shape resonance.

TABLE IV. $^4P^e$ resonance energies and width of He⁻ in the energy region near the He $(n=4)$ and He $(n=5)$ thresholds.

$_N(K,T)^A$	Present results $\hbar\omega$ (eV)	Γ (meV)	Label	Experiment[a] $\hbar\omega$ (eV)	Γ (meV)	Other theory $\hbar\omega$ (eV)	Γ (meV)
	3.544 676[b]					3.531 42 [c,d,b]	204.08[c,d]
$_4(2,1)^+$	3.810 432	27.7	**a**	3.8109(6)	30(2)	3.813 330[e,d]	23.48[e,d]
						3.811 38[f]	28.18[f]
						3.8057[c,d]	26.7[c,d]
$_4(2,1)^+$	3.946 404	5.7	**c**	3.946 63(3)	5.4(6)	3.947 54[f]	5.97[f]
						3.941 22[c,d]	6.5[c,d]
$_4(2,1)^+$	3.965 596	0.35	**e**	3.965 64(3)	0.33(5)	3.9614[c,d]	3.8[c,d]
$_4(0,1)^+$	3.982 388[b]	3.0	**f**	3.9822(2)	2.4(4)	3.994 01[c,d,b]	10.1[c,d]
$_4(0,1)^+$	3.993 956	0.01					
	3.994 054[b]						
$_5(3,1)^+$	4.168 788	22.5	**g**	4.167(5)	22(8)	4.168 248[e,d]	17.4[e,d]
						4.1376[f]	
						4.162 72[c,d]	21.8[c,d]
$_5(1,1)^+$	4.247 933	9.4	**h**	4.242(6)	11(8)		
$_5(3,1)^+$	4.257 047	5.6	**i**	4.257(1)	5(3)	4.254 15[c,d]	7.1[c,d]
$_5(3,1)^+$	4.280 228	2.5	**j**	4.2799(6)	3.2(6)	4.2770[c,d]	3.8[c,d]
	4.285 839		**k**	4.285 94(8)	0.25(8)	4.2825[c,d]	2.2[c,d]
$_5(1,1)^+$	4.294 182[b]	2.4	**l**	4.297(2)	4(4)	4.291 43[c,d,b]	18.5[c,d]
	4.298 986	0.4					
	4.300 279	0.1					
	4.300 537						

[a]I. Yu. Kiyan, U. Berzinsh, D. Hanstorp, and D. J. Pegg, Ref. [27].
[b]Shape resonance.
[c]M. Bylicki, Ref. [10].
[d]These values for the energies and widths are determined using the energy of He⁻ $(1s2s2p\ ^4P^o)$, $-2.177\,87725$ a.u., and the conversion factor 1 a.u.$= 27.211396$ eV.
[e]S. I. Themelis and C. A. Nicolaides, Ref. [7].
[f]J. Xi and C. Froese Fisher, Ref. [8].

TABLE V. $^4D^e$ resonance energies and widths of He$^-$ in the energy region near the He $(n=4)$ and He $(n=5)$ thresholds.

$_N(K,T)^A$	Present results $\hbar\omega$ (eV)	Γ (meV)
$_4(2,1)^+$	3.797 964	46.9
$_4(2,1)^+$	3.852 548	
	3.965 836	9.0
	3.973 010	10.6
	3.976 752	1.7
	3.991 757	0.2
	3.993 762	0.08
	3.993 860	0.02
$_5(3,1)^+$	4.156 931	112
$_5(4,0)^-$	4.206 487	3.4
$_5(1,1)^+$	4.228 976	0.8
$_5(3,1)^+$	4.252 719	8.9
$_5(2,2)^-$	4.268 700	1.3
$_5(2,0)^-$	4.271 526	0.9
$_5(3,1)^+$	4.278 547	7.1
	4.286 081	0.8
	4.286 524[a]	0.3
	4.291 919	1.1
	4.294 920	1.0
	4.297 999	0.3
	4.299 219	0.1
	4.299 904	0.1

[a]Shape resonance.

FIG. 13. $\sigma(3p, {}^4S^e)$ partial cross section in the vicinity of the He $(n=4)$ thresholds. (a) Present results in dipole velocity (length) approximation indicated by the solid (dotted) line. Results for $\sigma(3p, {}^4S^e)$ obtained by removing each of the following $^4S^e$ doubly excited states from the calculation are shown in (b)–(d): (b) Doubly excited state with symmetry $_N(K,T)^A = {}_4(3,0)^-$ at 3.814 225 eV. (c) Doubly excited state with symmetry $_N(K,T)^A = {}_4(3,0)^-$ at 3.851 397 eV. (d) Doubly excited state with symmetry $_N(K,T)^A = {}_4(1,0)^-$ at 3.951 457 eV. The vertical dashed lines indicate the locations of the He $(1snl\,{}^3l)$ thresholds. The arrows indicate the energy locations of the doubly excited state which has been removed from the cross-section result shown.

appears to be the resonance **b**. A second $^4S^e$ resonance is located just below the He $(1s4s\,{}^3S)$ threshold at 3.851 397 eV. The width of this resonance is probably too narrow to be observed experimentally. Brandefelt and Lindroth [13] showed a peak at the same position in their calculated $\sigma({}^4S^e)$ partial cross section from He$^-$ $(1s2s2p\,{}^4P^o)$, but its energy and width are not given. We find that these two $^4S^e$ doubly excited states have similar $nsn's$ configurations composition, and that their angular density plots show the same correlation pattern, indicating a $_N(K,T)^A = {}_4(3,0)^-$ character. While these ''$-$'' types of states appear as similarly narrow peaks in H$^-$ photodetachment spectra [51], such kinds of resonances in alkali negative ions are weak but not necessarily narrow [33,34]. Clearly the field of the He$^+$ $(1s)$ core is much closer to the Coulomb field of the H$^+$ core than are those of the singly ionized alkali atom cores. The third resonance, labeled as **d** in Ref. [27], is produced by a $^4S^e$ resonance located in our calculations at 3.951 457 eV, confirming the result of Brandefelt and Lindroth [13], who predicted a resonance energy of 3.951 58 eV. Owing to the strong contribution of the $4d6d$ and $4d5d$ configurations to the state responsible for this resonance, its density plot reveals a $_N(K,T)^A = {}_4(1,0)^-$ character, showing a nodal line in θ_{12} (equivalently, in λ) in the angular correlation pattern, which makes it qualitatively different from the other two $^4S^e$ states in this energy region. The density plots for these three $^4S^e$ doubly excited states in this energy region are given in Fig. 14.

Figure 12(c) shows a rich structure of $^4P^e$ resonances which dominate the $\sigma(3p, {}^4P^e)$ partial cross section. In the
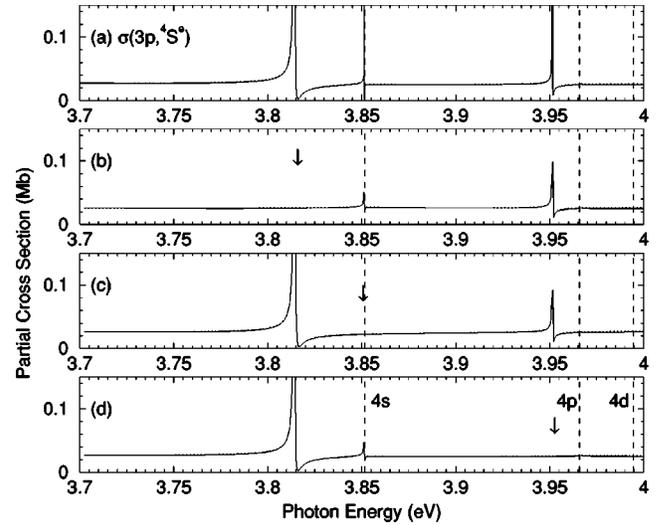
energy region shown in Fig. 12, while the eigenphase sum analysis reveals six $^4P^e$ resonances, we identify the five of them that are lowest in energy using our nonstandard projection operator method. Effects of each of the five $^4P^e$ resonances on the $\sigma(3p, {}^4P^e)$ partial cross section are shown in Fig. 15. A very broad ''$+$''-type doubly excited state located at 3.810 432 eV is responsible for the feature labeled as **a** in the experimental data [27]. A doubly excited state located at 3.946 404 eV produces the window resonance labeled as **c**. The very narrow window resonance **e** just below the He $(1s4p\,{}^3P)$ threshold is located at 3.965 596 eV. All three of these resonances below the He $(1s4p\,{}^3P)$ have the same angular correlation pattern, $_N(K,T)^A = {}_4(2,1)^+$, as well as similar $npn'p$ configuration compositions. This dominant series comprises the propensity rule allowed states, $_N(K,T)^A = {}_N(N-2,1)^+$ [52,53], which also dominate the photodetachment spectra of H$^-$ [52,31] and the alkali-metal negative ions [31–34]. The resonance feature labeled **f** in Ref. [27] is due to a doubly excited state located at 3.982 388 eV. Its angular correlation pattern indicates a $_N(K,T)^A = {}_4(0,1)^+$ character. While this state has dominant $nfn'f$ configuration components, it also has strong contributions from the $4p^2$ and $4p5p$ configurations. This result coincides with Bylicki's prediction of a shape resonance located at 3.994 01 eV [10]. However, while our predicted width agrees more or less with the experimental measurement [27], Bylicki's prediction is more than two times larger (cf. Table IV). An extremely narrow resonance located at 3.993 956 eV just below the He $(1s4d\,{}^3D)$ threshold is due to another $_N(K,T)^A = {}_4(0,1)^+$ doubly excited state.
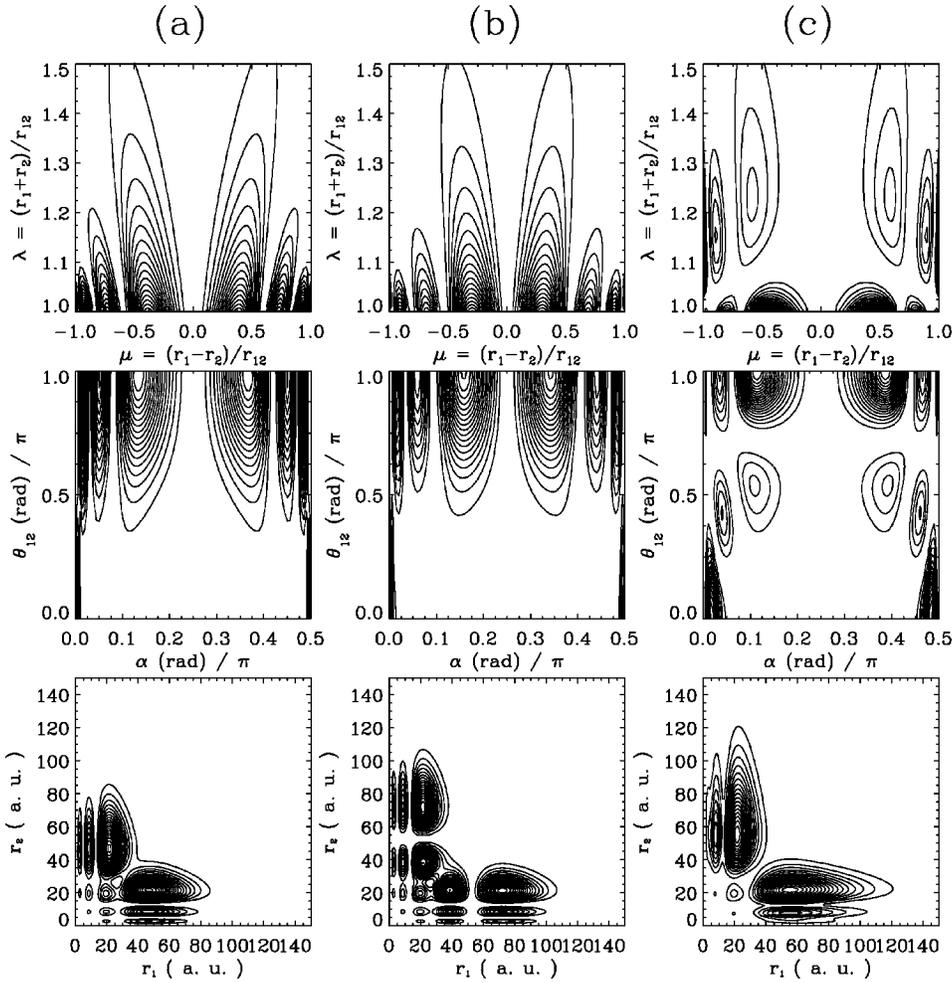
FIG. 14. Density plots for the $^4S^e$ resonance states near the He ($n=4$) thresholds. (a) $_4(3,0)^-$ state at $\hbar\omega = 3.814\,225$ eV. (b) $_4(3,0)^-$ state at $\hbar\omega = 3.851\,397$ eV. (c) $_4(1,0)^-$ state at $\hbar\omega = 3.951\,457$ eV. The density plots are as described in the caption to Fig. 11. The angular plots in the top and middle panels are plotted at the following radii: (a) $R=53$ a.u. (b) $R=45$ a.u. (c) $R=60$ a.u.

There also exist several $^4D^e$ resonances appearing in the $\sigma(3p,\,^4D^e)$ partial cross section in this energy region, as shown in Fig. 12(d), although few of them stand out as prominent features in the $\sigma(3p)$ partial cross section. To our knowledge, no $^4D^e$ resonance in this energy region has been studied previously, either theoretically or experimentally. Most of the eight resonances revealed by our eigenphase sum analysis in the neighborhood of He ($n=4$) thresholds are very weak features. Their energy locations and widths are given in Table V. However, due to the large number of such resonances appearing in this energy region, which spans three different thresholds, as well as the strong coupling between them, our nonstandard projection operator method has not been able to generate accurate doubly excited-state wave functions for those resonances located in the vicinity of the He ($1s4p\,^3P$) threshold. Nevertheless, we do identify two resonances below the He ($1s4s\,^3S$) threshold. The effect of each of the two resonances on the $\sigma(3p,\,^4D^e)$ partial cross section is shown in Fig. 16. A broad ''+''-type doubly excited state is located below the He ($1s4s\,^3S$) threshold at $3.797\,964$ eV. Since its position overlaps with the strong $^4P^e$ resonance labeled as **a**, this resonance is not identified by the experimental observation of the $\sigma(3p)$ partial cross section. Its density plot reveals a character of $_N(K,T)^A = {}_4(2,1)^+$. Our analysis indicates that the feature located at the He ($1s4s^3S$) threshold is a $^4D^e$ doubly excited resonance, having a photon energy position of $3.852\,548$ eV. (Because of its closeness to the threshold, we

are not able to predict a width for this resonance.) Our finding contradicts the statement in Ref. [27], which refers to this feature as a threshold ''cusp'' rather than as a resonance. Confirmation of this feature as a resonance is given in Fig. 16(c), which shows the effect on $\sigma(3p,\,^4D^e)$ of removing the doubly excited state we associate with this resonance. One sees that when this state is removed, $\sigma(3p,\,^4D^e)$ passes smoothly through the He ($1s4s\,^3S$) threshold, with no indication of any threshold cusp feature.

The $\sigma(3p,\,^4D^e)$ partial cross section indicates a large number of other resonances in the energy region between the He ($1s4p\,^3P$) and He ($1s4d\,^3D$) thresholds (cf. Table V). This contrasts with the absence of any $^4S^e$ resonance in this energy region. Although these $^4D^e$ resonances appear to be relatively weak features in $\sigma(3p)$, they are quite prominent in σ_{total} (cf. Fig. 2).

D. He⁻ photodetachment near the He ($n=5$) thresholds

We present our results in a way similar to that of Sec. III C. Figure 17(a) shows our calculated $\sigma(3p)$ partial cross section in the vicinity of the He ($n=5$) thresholds along with the experimental measurements [27]. The increased scatter of the experimental data in this energy region makes it difficult if not impossible to discern the weaker but more complex resonance features. The decomposition of the $\sigma(3p)$ partial cross section into the contributions $\sigma(3p,\,^4L^e)$ for each of the three different final-state orbital angular mo-
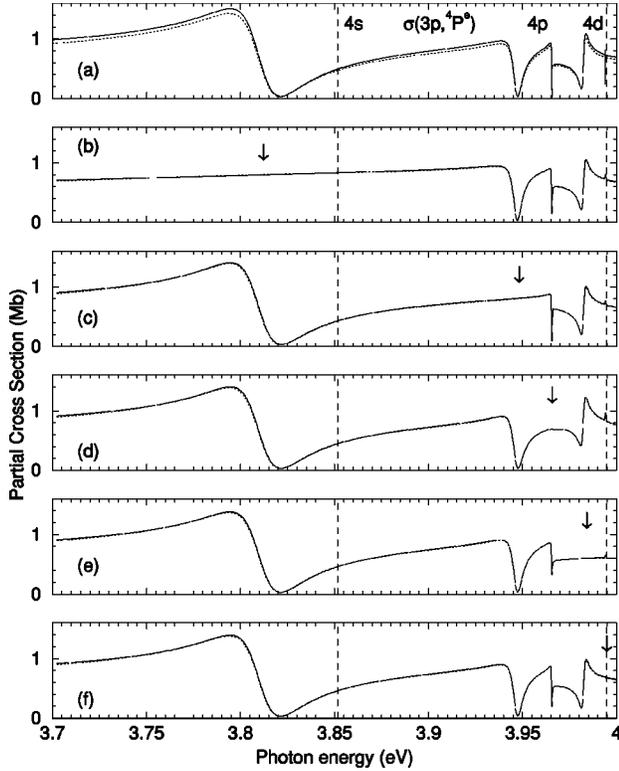
FIG. 15. $\sigma(3p, {}^4P^e)$ partial cross section in the vicinity of the He ($n=4$) thresholds. (a) Present results in dipole velocity (length) approximation indicated by the solid (dotted) line. Results for $\sigma(3p, {}^4P^e)$ obtained by removing each of the following ${}^4P^e$ doubly excited states from the calculation are shown in (b)–(f): (b) Doubly excited state with symmetry ${}_N(K,T)^A = {}_4(2,1)^+$ at 3.810 432 eV. (c) Doubly excited state with symmetry ${}_N(K,T)^A = {}_4(2,1)^+$ at 3.946 404 eV. (d) Doubly excited state with symmetry ${}_N(K,T)^A = {}_4(2,1)^+$ at 3.965 596 eV. (e) Doubly excited state with symmetry ${}_N(K,T)^A = {}_4(0,1)^+$ at 3.982 388 eV. (f) Doubly excited state with symmetry ${}_N(K,T)^A = {}_4(0,1)^+$ at 4.993 956 eV. The vertical dashed lines indicate the locations of the He ($1snl\ {}^3l$) thresholds. The arrows indicate the energy locations of the doubly excited state which has been removed from the cross-section result shown.

menta is presented in Figs. 17(b)–17(d). A large number of resonances are found in this energy region (cf. Tables III–V). Since the resonance structures become quite complex, especially in the energy regions very close to the thresholds, we only analyze here the most prominent resonance features. In this energy region, the contribution from the $\sigma(3p, {}^4S^e)$ partial cross section is almost negligible, as shown in Fig. 12(b), although the eigenphase sum analysis reveals as many as six resonances. One sees that the $\sigma(3p, {}^4P^e)$ partial cross section still dominates the $\sigma(3p)$ partial cross section and has a rich resonance structure, but the effects of the $\sigma(3p, {}^4D^e)$ partial cross section on $\sigma(3p)$ become more visible than they are near the He ($n=4$) thresholds. However, in the energy region between the He ($1s5s\ {}^3S$) and He ($1s5d\ {}^3D$) thresholds, the resonance features in $\sigma(3p, {}^4P^e)$ and $\sigma(3p, {}^4D^e)$ overlap, so that it is more difficult to identify the resonances from the composite $\sigma(3p)$ partial cross section than is the case near the He ($n=4$) thresholds. For example, the dip between the resonances **h** and **i** is deepened by the existence of a ${}^4D^e$ resonance located at 4.252 719 eV. Another example concerns the energy
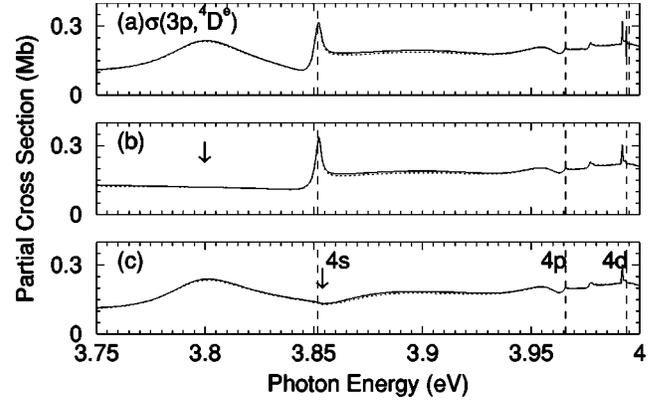

FIG. 16. $\sigma(3p, {}^4D^e)$ partial cross section in the vicinity of the He ($n=4$) thresholds. (a) Present results in dipole velocity (length) approximation indicated by the solid (dotted) line. Results for $\sigma(3p, {}^4D^e)$ obtained by removing each of the following ${}^4D^e$ doubly excited states from the calculation are shown in (b) and (c): (b) Doubly excited state with symmetry ${}_N(K,T)^A = {}_4(2,1)^+$ at 3.797 964 eV. (c) Doubly excited state with symmetry ${}_N(K,T)^A = {}_4(2,1)^+$ at 3.852 548 eV. The vertical dashed lines indicate the locations of the He ($1snl\ {}^3l$) thresholds. The arrows indicate the energy locations of the doubly excited state which has been removed from the cross-section result shown.

region between the He ($1s5p\ {}^3P$) and He ($1s5d\ {}^3D$) thresholds. While the experimental paper [27] identifies a resonance **l**, there are actually overlapping series of ${}^4P^e$ and ${}^4D^e$ resonances. In what follows, we discuss the most prominent ${}^4P^e$ and ${}^4D^e$ resonance features in this energy region.

While the eigenphase sum analysis reveals as many as nine ${}^4P^e$ resonances, our nonstandard projection operator method identifies five resonances in the energy region below the He ($1s5d\ {}^3D$) threshold. Effects of each of these five
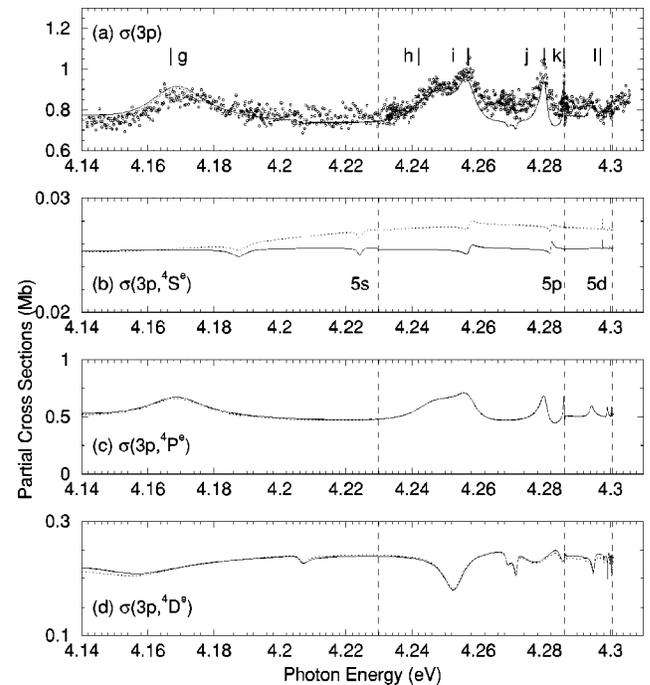

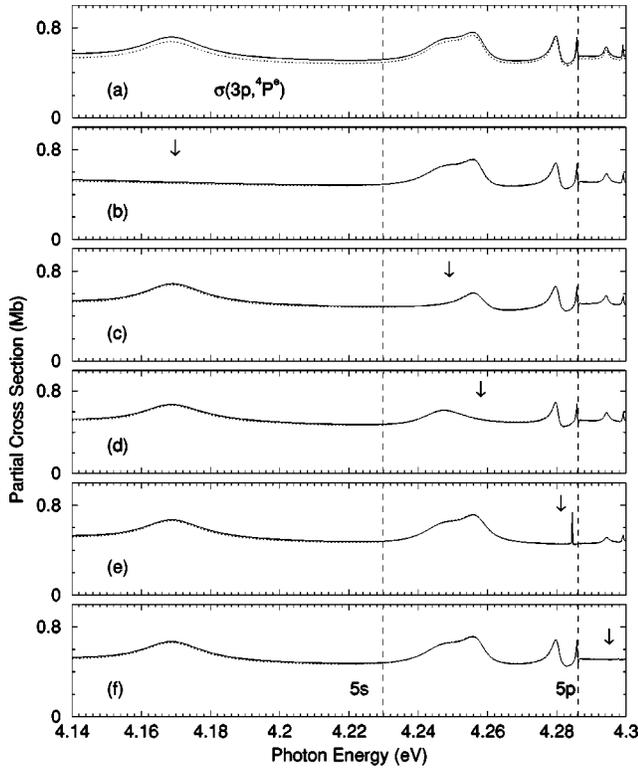FIG. 17. Same as in Fig. 12 in the energy region near the He ($n=5$) thresholds.

FIG. 18. $\sigma(3p, {}^4P^e)$ partial cross section in the vicinity of the He ($n=5$) thresholds. (a) Present results in dipole velocity (length) approximation indicated by the solid (dotted) line. Results for $\sigma(3p, {}^4P^e)$ obtained by removing each of the following ${}^4P^e$ doubly excited states from the calculation are shown in (b)–(f): (b) Doubly excited state with symmetry ${}_N(K,T)^A = {}_5(3,1)^+$ at 4.168 788 eV. (c) Doubly excited state with symmetry ${}_N(K,T)^A = {}_5(1,1)^+$ at 4.247 933 eV. (d) Doubly excited state with symmetry ${}_N(K,T)^A = {}_5(3,1)^+$ at 4.257 047 eV. (e) Doubly excited state with symmetry ${}_N(K,T)^A = {}_5(3,1)^+$ at 4.280 228 eV. (f) Doubly excited state with symmetry ${}_N(K,T)^A = {}_5(1,1)^+$ at 4.294 182 eV. The vertical dashed lines indicate the locations of the He ($1snl\ {}^3l$) thresholds. The arrows indicate the energy locations of the doubly excited state which has been removed from the cross-section result shown.

${}^4P^e$ doubly excited states are shown in Fig. 18. The resonance **g** located at 4.168 788 eV is due to a ${}^4P^e$ doubly excited state. Its density plot indicates a ${}_N(K,T)^A = {}_N(3,1)^+$ character, presenting another example of the dominant ${}_N(K,T)^A = {}_N(N-2,1)^+$ states. The experimentally observed resonances **h** and **i** overlap. Indeed, while a ${}_N(K,T)^A = {}_5(1,1)^+$ resonance located at 4.247 933 eV is responsible for feature **h**, a ${}_N(K,T)^A = {}_5(3,1)^+$ resonance located at 4.257 047 eV causes the second peak labeled **i**. Resonances **j** and **k** are very close to the He ($1s5p\ {}^3P$) threshold, implying that the corresponding doubly excited states have a very large spatial extent involving highly excited orbitals. Our analysis shows that the resonance **j** at 4.280 228 eV is produced by a ${}_N(K,T)^A = {}_5(3,1)^+$ state. The eigenphase sum analysis indicates a resonance at 4.285 839 eV, corresponding to resonance **k**. However, our nonstandard projection operator method is not able to generate the wave function of the corresponding doubly excited state because of the spatial limit of the R-matrix box. Figure 17(c) shows a much weaker series of ${}^4P^e$ resonances in the energy range between the He ($1s5p\ {}^3P$) and

He ($1s5d\ {}^3D$) thresholds, but the experimental data only identify one located at 4.297 eV and labeled **l**. In contrast, we predict that the most prominent resonance is located at 4.294 182 eV, and is produced by a ${}_N(K,T)^A = {}_5(1,1)^+$ doubly excited state. Also, while this state is dominated by $nfn'f$ configuration components, it has a strong contribution from the $5p7p$ and $5p8p$ configurations. This prediction also coincides with Bylicki's prediction of a shape resonance in this energy region, although our prediction does not agree with his predicted resonance energy at 4.291 43 eV. Also, in contrast to his prediction of a width of 18.5 meV, our predicted width of 2.4 meV is closer to the experimentally measured value of 4 meV [27]. However, the experimental data do not allow one to discern the weak resonance structures in this energy region or to distinguish between ${}^4P^e$ and ${}^4D^e$ resonances. Therefore identification of resonance **l** requires supporting theoretical analysis. It is worthwhile mentioning that the configuration compositions of each of the ${}^4P^e$ resonance states found in this energy region are strongly mixed. However, the leading configurations of these ${}_N(K,T)^A = {}_5(3,1)^+$ states are primarily mixtures of $npn'p$ and $ndn'd$ configurations, while the other two states with ${}_N(K,T)^A = {}_5(1,1)^+$ have strong $nfn'f$ components.

The ${}^4D^e$ resonances become relatively prominent in this energy region, as compared with the dominant ${}^4P^e$ ones, although few of their features are observed in the $\sigma(3p)$ partial cross section. Figure 19 shows the effects of each of the seven doubly excited states below the He ($1s5p\ {}^3P$) threshold that we obtained by our nonstandard projection operator method. A doubly excited state is responsible for the broad resonance at 4.156 931 eV, just below the position of the experimentally observed resonance **g**. Its angular correlation pattern clearly indicates a ${}_N(K,T)^A = {}_5(3,1)^+$ state. The small resonance dip at 4.206 487 eV is produced by a ${}_N(K,T)^A = {}_5(4,0)^-$ state. A doubly excited resonance located at 4.228 976 almost does not affect the cross section at all, as shown in Fig. 19(c): its removal from our final state only slightly broadens the window resonance at 4.252 719 eV, as may be seen by comparing Figs. 18(a) and 18(c). Its angular density plots reveal a ${}_N(K,T)^A = {}_5(1,1)^+$ character. Such a state is also found to have minimal effects on the cross sections in both H$^-$ and Li$^-$ photodetachment [54]. The window resonance at a photon energy of 4.252 719 eV corresponds to a ${}_N(K,T)^A = {}_5(3,1)^+$ doubly excited state; it causes a deeper dip between the resonance features **h** and **i** (discussed above) in the $\sigma(3p)$ partial cross section. The double-dip feature near a photon energy of 4.27 eV is caused by two overlapping, doubly excited-state resonances. However, the experimental data does not have enough resolution to observe this feature. One resonance is located at 4.268 700 eV; its angular correlation indicates a ${}_N(K,T)^A = {}_5(2,2)^-$ character. Another one is located at 4.271 526 eV and has a ${}_N(K,T)^A = {}_5(2,0)^-$ character. The former does not exist in either H$^-$ or in alkali-metal negative ion spectra, for which the final state has only the term value ${}^1P^o$. The latter character is predicted to occur in both systems, but its effects are only observed in alkali-metal negative ions and not in H$^-$ [33], implying that its observation requires a nonhydrogenic core. Figure 20 presents density plots for each of the three ${}^4D^e$ doubly excited states having ''$-$'' character.
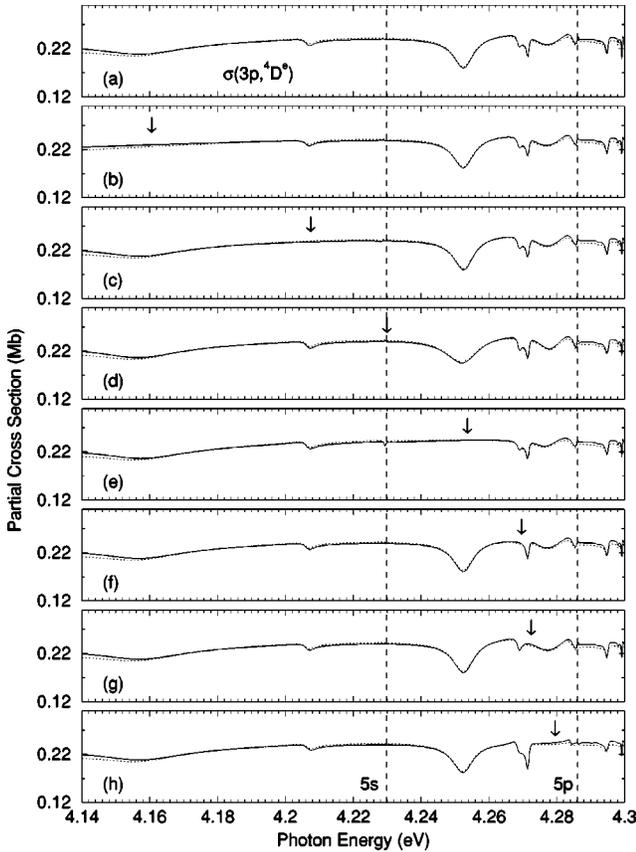
FIG. 19. $\sigma(3p, {}^4D^e)$ partial cross section in the vicinity of the He $(n=5)$ thresholds. (a) Present results in dipole velocity (length) approximation indicated by the solid (dotted) line. Results for $\sigma(3p, {}^4D^e)$ obtained by removing each of the following ${}^4D^e$ doubly excited states from the calculation are shown in (b)–(g): (b) Doubly excited state with symmetry ${}_N(K,T)^A = {}_5(3,1)^+$ at 4.156 931 eV. (c) Doubly excited state with symmetry ${}_N(K,T)^A = {}_5(4,0)^-$ at 4.206 487 eV. (d) Doubly excited state with symmetry ${}_N(K,T)^A = {}_5(1,1)^+$ at 4.229 976 eV. (e) Doubly excited state with symmetry ${}_N(K,T)^A = {}_5(3,1)^+$ at 4.252 719 eV. (f) Doubly excited state with symmetry ${}_N(K,T)^A = {}_5(2,2)^-$ at 4.268 700 eV. (g) Doubly excited state with symmetry ${}_N(K,T)^A = {}_5(2,0)^-$ at 4.271 526 eV. (h) Doubly excited state with symmetry ${}_N(K,T)^A = {}_5(3,1)^+$ at 4.278 547 eV. The vertical dashed lines indicate the locations of the He $(1snl\ {}^3l)$ thresholds. The arrows indicate the energy locations of the doubly excited state which has been removed from the cross-section result shown.

IV. DISCUSSION

Complete lists of energies and widths (when possible) for our predicted ${}^4S^e$, ${}^4P^e$, and ${}^4D^e$ resonances in the energy region of the He $(n=3, 4,$ and $5)$ thresholds are presented in Tables II–V, together with prior theoretical and experimental results. A large number of these resonances are reported here for the first time. Agreement between our predictions and the recent experimental measurements for He$^-$ photodetachment partial cross sections [25–27] is excellent. Most prior theoretical and experimental predictions focused on ${}^4P^e$ resonances. However, since experimental measurements of partial cross sections cannot definitely identify the term values of these resonances, our predictions for the decomposition of the partial cross sections into components of different total orbital angular momenta provides important information.

While most prior theoretically predicted resonances are located below the He $(1snp\ {}^3P)$ thresholds, except for the three ${}^4P^e$ shape resonances predicted by Bylicki [10], we find that resonance structures also exist below the He $(1snd\ {}^3D)$ thresholds for $n \geqslant 4$, although most of these resonances are too weak or too narrow to be observed by the most recent experimental measurements [27]. Besides predicting several additional ${}^4P^e$ resonances that have not been reported before, we also predict a large number of ${}^4S^e$ and ${}^4D^e$ resonances that have not been either predicted or observed. The ${}^4S^e$ resonances in the energy region above the He $(n=4)$ thresholds are narrow and relatively weak, so it is not easy to observe them experimentally if the measured partial cross section is dominated by ${}^4P^e$ or ${}^4D^e$ resonances . In the energy region considered in this paper, the ${}^4D^e$ resonances are not clearly observed in $\sigma(3p)$ because they are overshadowed by the prominent ${}^4P^e$ resonances. The best way to observe the ${}^4S^e$ and ${}^4D^e$ resonances is to measure the $\sigma(ns)$ partial cross sections for high n since these partial cross sections have no $\sigma(ns, {}^4P^e)$ components.

Characterization of resonance structures is an increasingly difficult problem the higher the excitation energy one treats. In the energy region of the He $(n=3, 4,$ and 5$)$ thresholds, our nonstandard projection operator method provides an accurate representation of the doubly excited states responsible for the resonance features in the photodetachment partial cross sections and in the photoelectron angular distributions. In all cases, doubly excited states show strong configuration mixing, reflecting the complexity of electron correlations and the importance of channel interactions. The approximate quantum number notations derived by various classification schemes [42–46] provide more insight into topological properties of the two-electron wave function and, therefore, are better descriptions of the states than the commonly used single-configuration designations.

Compared with the total cross section, the partial cross sections show much more complex resonance structures. While many resonances show minute effects on the total cross section, they show strong interference effects such as asymmetric peaks and nearly zero minima in the partial cross sections associated with high levels of excitation of the residual atom. Therefore, partial cross sections are more sensitive to the doubly excited resonances, and thus are better candidates for studies of doubly excited-state resonances. From the results presented here, it appears also that partial cross sections corresponding to higher levels of excitation of the residual atom show such effects more prominently than those for lower levels of atomic excitation. Precisely because highly excited, doubly excited resonances have only a small effect on the total cross section (i.e., their ρ^2 parameter [47] is nearly zero), mirroring behavior is commonly observed between their profiles in different partial cross sections [30], as we have shown here for ${}^4S^e$ doubly excited states in the vicinity of the He $(n=5)$ thresholds (cf. Figs. 4 and 5). In contrast to such mirroring behavior, partial cross sections exhibit *in-phase* variations near any deep window resonance in the total cross section (i.e., when ρ^2 is close to 1), as we prove analytically in the Appendix. This behavior is illustrated by the $\sigma(nl, {}^4P^e)$ partial cross sections in the neighborhood of the three ${}^4P^e$ window resonances below the He $(1s4p\ {}^3P)$ threshold, which produce nearly zero minima

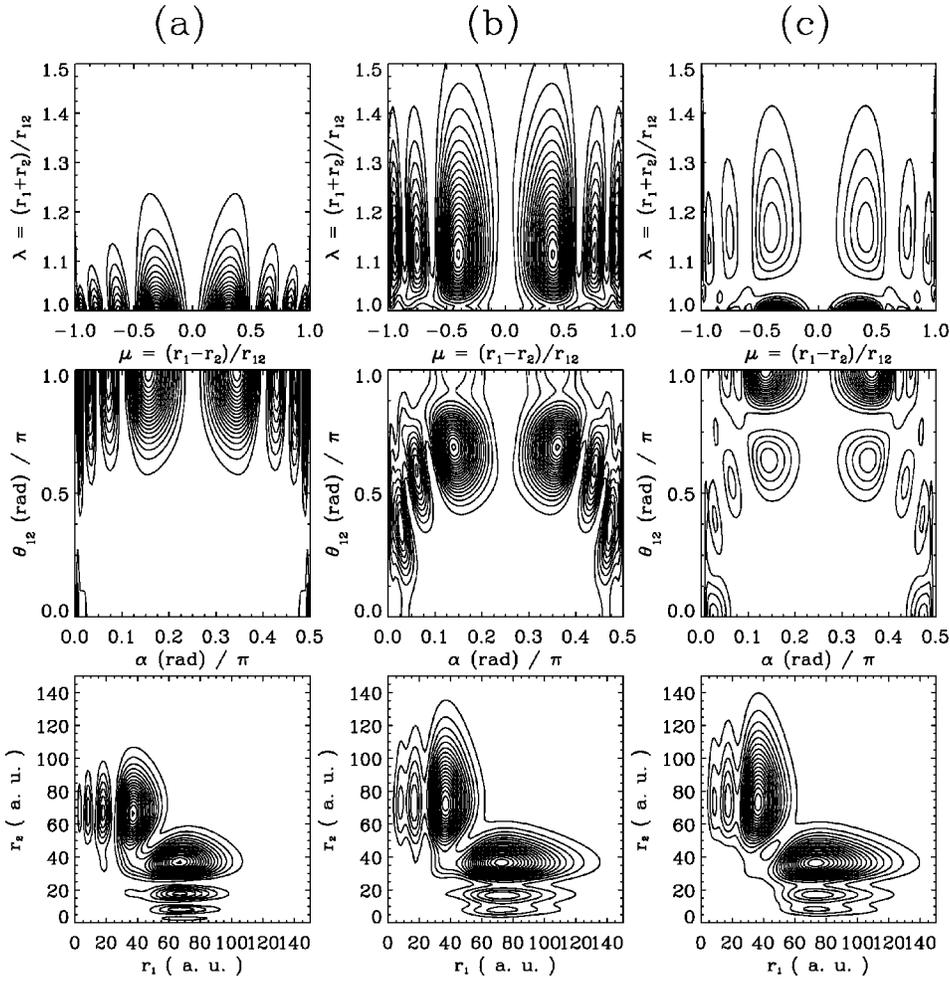FIG. 20. Density plots for three $^4D^e$ resonance states in the vicinity of the He ($n=5$) thresholds. (a) $_5(4,0)^-$ state at $\hbar\omega = 4.206\,487$ eV. (b) $_5(2,2)^-$ state at $\hbar\omega = 4.268\,700$ eV. (c) $_5(2,0)^-$ state at $\hbar\omega = 4.271\,526$ eV. The density plots are described in the caption to Fig. 11. The angular plots in the top and middle panels are plotted at the following radii: (a) $R=78$ a.u. (b) $R=83$ a.u. (c) 81 a.u.

in the $\sigma(^4P^e)$ partial cross section.

Based on the observation that states of given total symmetry are built on a single molecular orbital in the adiabatic molecular-orbital description of exact two-electron systems (i.e., H⁻ and He), propensity rules for radiative and nonradiative transitions are derived according to selection rules that govern the transitions between states associated with different molecular orbitals [53,55]. These propensity rules have proved successful in explaining characteristics of different $_N(K,T)^A$ resonance series of doubly excited He [56,57], which has been studied in great detail. Since the mechanism of autoionization depends on the non-adiabatic transition between different molecular orbitals, propensity rules for nonradiative transitions shed light on the variation of resonance widths [55,57]. In general, states with $A=+$ have larger widths than those with $A=-$. Also, among all series having the same quantum number A, series with larger K have larger widths because there are more continua into which these states can decay [55,57]. Our results for He⁻ are consistent with these propensity rules. For example, comparing the most prominent states of each A symmetry for the same N, the width of the $_4(2,1)^+$ $^4P^e$ resonance (cf. Table IV) is about 34 times larger than that of the $_4(3,0)^-$ $^4S^e$ resonance (cf. Table III). Comparing states of different K values, the width of the $_5(3,1)^+$ $^4D^e$ resonance is 140 times larger than that of the $_5(1,1)^+$ $^4D^e$ resonance, and the $_5(4,0)^-$ $^4D^e$ resonance also has a width almost four times larger than the $_5(2,0)^-$ $^4D^e$ resonance (cf. Table V).

Propensity rules for radiative transitions are derived by analysis of the dipole matrix elements using a saddle-point approximation as well as the symmetries of the corresponding resonance states, both of which govern the strength of transition from the ground state to prospective resonance states [46,53]. These rules can be expressed in the form, $\Delta v_2 = 0, \pm 1$, where v_2, defined as $N-K-1$, is a quantum number of the Hamiltonian resulting from the saddle-point dynamics [46]. Because the He⁺ core only slightly perturbs the two outer electrons, the same classification schemes and propensity rules for H⁻ and He also apply to He⁻ [4]. Given the symmetry of the He⁻ initial state, $_N(K,T)^A = _2(1,0)^+$, the dominant final-state resonances (as predicted by the dipole transition propensity rules) are $_N(K,T)^A = _N(N-2,1)^+$ for $^4P^e$ and $^4D^e$ (i.e., $\Delta v_2 = +1$) and $_N(K,T)^A = _N(N-1,0)^-$ for $^4S^e$ (i.e., $\Delta v_2 = 0$) [53]. For H⁻ [51,52] and He [56,57], the $_N(N-2,1)^+$ series, referred to as the *principal series*, contains the dominant resonances. The $_N(N-1,0)^-$ series is the secondmost prominent series in H⁻, producing weaker and narrower resonances [51]. In contrast with H⁻, this series is weaker than the $_N(N-4,1)^+$ series in He [56,57]. Nevertheless, the $_N(N-1,0)^-$ resonances are quite broad in the spectra of the negative alkali-metal ions [33,34]. For He⁻, most of the prominent $^4P^e$ and $^4D^e$ resonances belong to the principal series, showing relatively broader and stronger features. Since $^4S^e$ can have only $T=0$ states, $_N(K,T)^A = _N(N-1,0)^-$ states are the only ones that satisfy the dipole transition propensity rule, and hence they are

much narrower resonances due to their ''$-$'' character. Both $^4S^e$ resonances below the He ($1s4s\,^3S$) threshold belong to this category: they have large dipole transition probabilities, but have very narrow widths. In contrast, for $^4P^e$ symmetry, no such $_N(N-1,0)^-$ state is predicted (cf. Table IV). Two such states are predicted with $^4D^e$ symmetry: the one in the vicinity of the He ($n=5$) thresholds (cf. Table V) has a negligible effect on the partial cross sections [cf. Fig. 19(c)]; in contrast, the second $^4D^e$ resonance we predicted near the He ($n=3$) thresholds is also of this type and is considerably more prominent (cf. Fig. 9). In addition to these two propensity-favored series, there are less prominent series of both ''$+$'' and ''$-$'' states appearing in the He$^-$ spectrum. These series have narrower widths and weaker transition amplitudes from the ground state compared with the principal series. The $_N(K,T)^A = _N(N-4,1)^+$ series in the $\sigma(^4P^e)$ and $\sigma(^4D^e)$ partial cross sections are relatively much more prominent in He$^-$ photodetachment (cf. Fig. 2) than are states of the same series in He photoionization [56]. While this series is the secondmost dominant one in He photoionization, this series has little effect on the partial cross section for H$^-$ photodetachment. A secondary series in the $\sigma(^4S^e)$ partial cross sections is the $_N(K,T)^A = _N(N-3,0)^-$ series, which also produces weaker, but nevertheless visible, resonances (cf. Fig. 2). In summary, the major resonance structures in He$^-$ photodetachment are consistent with the propensity rules derived for purely two-electron systems, such as H$^-$ and He.

V. CONCLUSIONS

We have presented a comprehensive theoretical study for He$^-$ photodetachment over the energy region of the He ($n = 3, 4,$ and 5) thresholds, including theoretical predictions for the $\sigma(3p)$ partial cross section. Predictions have also been given for total and partial cross sections corresponding to different total orbital angular momenta in order to facilitate identification of resonance structures. Characterization and identification of our predicted resonance structures have required numerous subsidiary calculations. We have used two different approaches for obtaining resonance energies and widths: (1) fitting the partial cross sections to a resonance profile formula, when the resonances are isolated; or (2) analyzing the eigenphase sum, when resonances are overlapping. To obtain configuration interaction representations for the doubly excited states, we have used a nonstandard projection operator method. These representations show that the resonances in the energy region we consider here cannot be described by a single dominant configuration. Rather we have made density plots of these resonance states to reveal their $_N(K,T)^A$ symmetries. We have also checked the accuracy of our representations by orthogonalizing our final-state photodetachment wavefunctions to these doubly excited states. In all cases, as we have shown, this orthogonalization procedure results in the associated resonance feature being completely removed from the partial cross section, thereby confirming the accuracy of our doubly excited-state representations. While our results confirm most of the resonances observed in recent experiments [25–27], we predict additional resonances that have not been either theoretically predicted or experimentally observed. For the two new $^4D^e$

resonances we predict near the He ($n=3$) thresholds, we have also predicted the effects of these resonances on partial cross sections and on photoelectron angular distribution asymmetry parameters.

We have shown that alternative partial cross sections for He ($1snl\,^3l$) states generally tend to mirror each other in the vicinity of a resonance, confirming our analytical prediction [30] for resonances characterized by $\rho^2 \rightarrow 0$. However, we have found three $^4P^e$ resonances that are exceptional, having ρ^2 close to unity, its maximum value. We prove analytically in the Appendix that partial cross sections in the vicinity of such resonances mimic each other by exhibiting identical energy variations, and we have confirmed this prediction using our calculated partial cross section results.

The major resonance structures in the total cross section have been found to reflect propensity rules for radiative and non-radiative transitions. The principal series of resonances, having $_N(K,T)^A = _N(N-2,1)^+$, fulfills the condition for propensity-favored transitions. Members of this series with $^4P^e$ and $^4D^e$ symmetries generally exhibit stronger transition amplitudes and broader widths. The propensity-allowed series with $^4S^e$ symmetry, having $_N(K,T)^A = _N(N-1,0)^-$, also exhibit strong transition amplitudes, but they are generally narrow due to their ''$-$'' character. Secondary series of resonances, such as $_N(N-4,1)^+$, and $_N(N-3,0)^-$, are also prominent in the He$^-$ photodetachment spectrum. Although such states have little effect in H$^-$ photodetachment, the $_N(N-4,1)^+$ series is the secondmost prominent one in He photoionization.

We have compared our results on the He$^-$ photodetachment spectrum in the energy region near the He ($n=3, 4,$ and 5) thresholds as well as on the doubly excited resonances in the spectrum with all prior theoretical and experimental work known to us. While our results are in excellent agreement with the experimental measurements of Ref. [25–27], a large number of resonances are predicted here for the first time. In particular, since no prior experimental observation of $^4D^e$ resonances has been reported, we suggest here how they may be observed experimentally.

APPENDIX: MIMICKING BEHAVIOR OF PARTIAL CROSS SECTION RESONANCE PROFILES WHEN $\rho^2 \rightarrow 1$

Our analysis is based upon a few key formulas from Ref. [39]. The main one is for the ratio of two partial cross sections in the vicinity of an isolated resonance, given by Eq. (43) of Ref. [39]. We write that result here for two groups of partial cross sections, denoted by P and Q:

$$\sigma_P = \frac{\sigma_P^0}{1+\epsilon^2}\{\epsilon^2 + 2\epsilon C_1 + (1+C_2)\}, \qquad \text{(A1)}$$

$$\sigma_Q = \frac{\sigma_Q^0}{1+\epsilon^2}\{\epsilon^2 + 2\epsilon[q\rho^2(1+r)-rC_1]$$

$$+[1+(q^2-1)\rho^2(1+r)-rC_2)]\}, \qquad \text{(A2)}$$

where

$$r \equiv (\sigma_P^0/\sigma_Q^0)_0, \qquad \text{(A3)}$$

$$C_1 \equiv q\,\mathrm{Re}\langle\alpha\rangle_P - \mathrm{Im}\langle\alpha\rangle_P, \qquad \text{(A4)}$$

$$C_2 \equiv (q^2+1)\langle|\alpha|^2\rangle_P - 2q\,\mathrm{Im}\langle\alpha\rangle_P - 2\,\mathrm{Re}\langle\alpha\rangle_P. \qquad \text{(A5)}$$

In Eqs. (A1)–(A5), σ_P^0 and σ_Q^0 are partial cross sections in the absence of the resonance, ϵ and q are the well-known Fano profile variables [37], which come from his analysis of the total cross section, and $\sigma_{TOT} = \sigma_P + \sigma_Q$, and $\langle\alpha\rangle_P$ and $\langle|\alpha|^2\rangle_P$ are parameters introduced by Starace [39] to describe the effects of a resonance on a partial cross section.

C_1 and C_2 can be further parametrized as in Eq. (52) of Ref. [39]:

$$C_1 \equiv \frac{R}{(1+r)^{1/2}}\sin\theta\sin\phi + q\rho^2, \qquad \text{(A6)}$$

$$C_2 \equiv -1 + R^2\sin^2\theta\cos^2\phi + C_1^2, \qquad \text{(A7)}$$

where θ and ϕ are parametric variables and

$$R^2 \equiv \left(1+\frac{1}{r}\right)[1+(q^2-1)\rho^2 - q^2\rho^4]. \qquad \text{(A8)}$$

From Eq. (A8), $R\to 0$ as $\rho^2\to 1$. From Eq. (A6), one then has $C_1 = q$ and $C_2 = q^2 - 1$. Then

$$\frac{\sigma_P}{\sigma_P^0} = \frac{\sigma_Q}{\sigma_Q^0} = \frac{(\epsilon+q)^2}{1+\epsilon^2} \qquad \text{(A9)}$$

Since the division of the total cross section into groups P and Q is arbitrary, one sees that each partial cross section has the same energy dependence in the neighborhood of a resonance for which $\rho^2\to 1$.

[1] E. Holøien and J. Midtdal, Proc. Phys. Soc. London, Sect. A **68**, 815 (1955).

[2] See, for example, P. Kristensen, U.V. Pedersen, V.V. Petrunin, T. Andersen, and K.T. Chung, Phys. Rev. A **55**, 978 (1997), and references therein.

[3] C.A. Nicolaides, Y. Komninos, and D. Beck, Phys. Rev. A **24**, 1103 (1981).

[4] S. Watanabe, Phys. Rev. A **25**, 2074 (1982).

[5] B.F. Davis, and K.T. Chung, Phys. Rev. A **41**, 5844 (1990).

[6] M. Le Dourneuf, and S. Watanabe, J. Phys. B **23**, 3205 (1990).

[7] S.I. Themelis and C.A. Nicolaides, J. Phys. B **28**, L379 (1995).

[8] J. Xi and C. Froese Fischer, Phys. Rev. A **53**, 3169 (1996).

[9] D. Kim, H.-L. Zhou, and S.T. Manson, J. Phys. B **30**, L1 (1997); Phys. Rev. A **55**, 414 (1997).

[10] M. Bylicki, J. Phys. B **30**, 189 (1997).

[11] K.T. Chung, Phys. Rev. A **58**, 2777 (1998).

[12] J. Xi and C. Froese Fischer, Phys. Rev. A **59**, 307 (1999).

[13] N. Brandefelt and E. Lindroth, Phys. Rev. A **59**, 2691 (1999).

[14] C.A. Ramsbottom and K.L. Bell, J. Phys. B **32**, 1315 (1999).

[15] A.U. Hazi and K. Reed, Phys. Rev. A **24**, 2269 (1981).

[16] L.V. Chernysheva, G.F. Gribakin, V.K. Ivanov, and M. Yu Kuchiev, J. Phys. B **21**, L419 (1988).

[17] H.P. Saha and R.N. Compton, Phys. Rev. Lett. **64**, 1510 (1990).

[18] V.K. Ivanov, G.Yu. Kashenock, G.F. Gribakin, and A.A. Gribakina, J. Phys. B **29**, 2669 (1996).

[19] R.V. Hodges, M.J. Coggiola, and J.R. Peterson, Phys. Rev. A **23**, 59 (1981).

[20] R.N. Compton, G.D. Alton, and D.J. Pegg, J. Phys. B **13**, L651 (1980).

[21] J.R. Peterson, M.J. Coggiola, and Y.K. Bae, Phys. Rev. Lett. **50**, 664 (1983).

[22] J.R. Peterson, Y.K. Bae, and D.L. Huestis, Phys. Rev. Lett. **55**, 692 (1985).

[23] D.J. Pegg, J.S. Thompson, J. Dellwo, R.N. Compton, and G.D. Alton, Phys. Rev. Lett. **64**, 278 (1990).

[24] C.W. Walter, J.A. Seifert, and J.R. Peterson, Phys. Rev. A **50**, 2257 (1994).

[25] A.E. Klinkmüller, G. Haeffler, D. Hanstorp, I.Yu. Kiyan, U. Berzinsh, C.W. Ingram, D.J. Pegg, and J.R. Peterson, Phys. Rev. A **56**, 2788 (1997).

[26] A.E. Klinkmüller, G. Haeffler, D. Hanstorp, I.Yu. Kiyan, U. Berzinsh, and D.J. Pegg, J. Phys. B **31**, 2549 (1998).

[27] I.Yu. Kiyan, U. Berzinsh, D. Hanstorp, and D.J. Pegg, Phys. Rev. Lett. **81**, 2874 (1998).

[28] U. Fano and C.M. Lee, Phys. Rev. Lett. **31**, 1573 (1973).

[29] P.F. O'Mahony and C.H. Greene, Phys. Rev. A **31**, 250 (1985); C.H. Greene and L. Kim, *ibid.* **36**, 2706 (1987); C.H. Greene, in *Fundamental Processes of Atomic Dynamics*, edited by J.S. Briggs, H. Kleinpoppen, and H.O. Lutz (Plenum, New York, 1988), pp. 105–127.

[30] C.N. Liu and A.F. Starace, Phys. Rev. A **59**, R1731 (1999).

[31] C. Pan, A.F. Starace, and C.H. Greene, J. Phys. B **27**, L137 (1994).

[32] C. Pan, A.F. Starace, and C.H. Greene, Phys. Rev. A **53**, 840 (1996).

[33] C.N. Liu and A.F. Starace, Phys. Rev. A **58**, 4997 (1998).

[34] C.N. Liu and A.F. Starace, Phys. Rev. A **59**, 3643 (1999).

[35] B.H. Bransden and C.J. Joachian, *Physics of Atoms and Molecules* (Addison-Wesley Longman Ltd., Harlow, England, 1983), p. 227.

[36] *Atomic Energy Levels*, edited by C.E. Moore, Natl. Bur. Stand. (U.S.) Circ. No. NSRDS-NBS35 (U.S. GPO, Washington, DC, 1971).

[37] U. Fano, Phys. Rev. **124**, 1866 (1961).

[38] B.W. Shore, Phys. Rev. **171**, 43 (1968).

[39] A.F. Starace, Phys. Rev. A **16**, 231 (1977).

[40] R.K. Nesbet and J.D. Lyons, Phys. Rev. A **4**, 1812 (1971).

[41] A.U. Hazi, Phys. Rev. A **19**, 920 (1979).

[42] D.R. Herrick, Phys. Rev. A **12**, 413 (1975); Adv. Chem. Phys. **52**, 1 (1983).

[43] C.D. Lin, Phys. Rev. A **29**, 1019 (1984); Adv. At. Mol. Phys. **22**, 77 (1986).

CHIEN-NAN LIU AND ANTHONY F. STARACE

PRA 60

[44] J.M. Feagin and J.S. Briggs, Phys. Rev. Lett. **57**, 984 (1986); Phys. Rev. A **37**, 4599 (1988).

[45] J.M. Rost, R. Gersbacker, K. Richter, J.S. Briggs, and D. Wintgen, J. Phys. B **24**, 2455 (1991).

[46] J.M. Rost and J.S. Briggs, J. Phys. B **24**, 4293 (1991).

[47] U. Fano and J.W. Cooper, Phys. Rev. **137**, A1364 (1965); Rev. Mod. Phys. **40**, 441 (1968), Sec. 8. 1.

[48] R.S. Oberoi and R.K. Nesbet, Phys. Rev. A **8**, 2969 (1973).

[49] P.G. Burke, Adv. At. Mol. Phys. **4**, 173 (1968).

[50] C.A. Nicolaides, N.A. Piangos, and Y. Komninos, Phys. Rev. A **48**, 3578 (1993), cf. Sec. VI.

[51] See, for example, J.Z. Tang, and I. Shimamura, Phys. Rev. A **51**, R1738 (1995), and references therein.

[52] H.R. Sadeghpour and C.H. Greene, Phys. Rev. Lett. **65**, 313 (1990); H.R. Sadeghpour, Phys. Rev. A **43**, 5821 (1991).

[53] A. Vollweiter, J.M. Rost, and J.S. Briggs, J. Phys. B **24**, L115 (1991).

[54] C. N. Liu, Ph.D. thesis, University of Nebraska–Lincoln, 1999.

[55] J.M. Rost and J.S. Briggs, J. Phys. B **23**, L339 (1990).

[56] M. Domke, K. Schulz, G. Remmers, G. Kaindl, and D. Wintgen, Phys. Rev. A **53**, 1424 (1996).

[57] J.M. Rost, K. Schulz, M. Domke, and G. Kaindl, J. Phys. B **30**, 4663 (1997).